Lack of Oncomodulin Increases ATP-Dependent Calcium Signaling and Susceptibility to Noise in Adult Mice

Yang Yang[1], Jing-Yi Jeng[2], Kaitlin Murtha[1], Leslie K. Climer[1], Federico Ceriani[2], Weintari D. Sese[1], Aubrey J. Hornak[1], M. Charles Liberman[6,7], Walter Marcotti[2,4], Dwayne D. Simmons[1,2,3,5,#]

[1]Department of Biology, Baylor University, 101 Bagby Ave, Waco, TX
[2]School of Biosciences, University of Sheffield, S10 2TN Sheffield, United Kingdom
[3]Department of Integrative Biology and Physiology, University of California, Los Angeles, CA
[4]Sheffield Neuroscience Institute, University of Sheffield, Sheffield, S10 2TN, UK
[5]Department of Psychology and Neuroscience, Baylor University, Waco, TX
[6]Department of Otolaryngoloy, Head & Neck Surgery. Harvard Medical School, Boston, MA
[7]Eaton-Peabody Laboratories, Mass Eye and Ear, Boston, MA
[#]To whom correspondence should be addressed: dwayne_simmons@baylor.edu

Keywords:

EF-hand calcium-binding protein (CaBP)
GCaMP6s
Noise-induced hearing loss
Oncomodulin (OCM)
Outer Hair Cell (OHC)
Purinergic receptor

Abstract

Tight regulation of Ca^{2+} is crucial for the function of cochlear outer hair cells (OHCs). Dysregulation of Ca^{2+} homeostasis in OHCs is associated with impaired hearing function and contributes to increased vulnerability to environmental insults, such as noise exposure. Ca^{2+} signaling in developing OHCs can be modulated by oncomodulin (OCM), an EF-hand calcium-binding protein. Here, we investigated whether the lack of OCM disrupts the control of intracellular Ca^{2+} in mature OHCs, and influences vulnerability to noise. Using young adult CBA/CaJ mice, we found that OHCs from *Ocm*-knockout (*Ocm*$^{-/-}$) mice exhibited normal biophysical profiles and electromotile responses compared to littermate control OHCs. Moderate noise exposure (95 dB SPL, 2 hrs) caused temporary hearing threshold shifts in *Ocm*$^{+/+}$ and *Ocm*$^{-/-}$ mice but the loss of hearing was permanent for *Ocm*$^{-/-}$ mice. However, while *Ocm*$^{+/+}$ fully recovered their hearing 2 weeks after noise exposure, *Ocm*$^{-/-}$ mice showed permanent threshold shifts. Using a genetically encoded Ca^{2+} sensor (GCaMP6s) expressed in *Ocm*$^{+/+}$ and *Ocm*$^{-/-}$ OHCs, we found that chronic noise exposure (95 dB SPL, 9 hrs) increased ATP-induced Ca^{2+} signaling in *Ocm*$^{-/-}$ OHCs compared to *Ocm*$^{+/+}$ OHCs. Chronic noise exposures also caused higher hearing threshold shifts in *Ocm*$^{-/-}$ mice. Prior to noise exposure, P2X2 expression was already upregulated in *Ocm*$^{-/-}$ mice compared to *Ocm*$^{+/+}$ mice. Following chronic noise, P2X2 receptors were upregulated in the *Ocm*$^{+/+}$ cochlea but not in the *Ocm*$^{-/-}$ cochlea, which retains their pre-noise high expression level. We propose that the lack of OCM increases susceptibility to noise. Increased purinergic signaling and dysregulation of cytosolic Ca^{2+} homeostasis could contribute to early onset hearing loss in the *Ocm*$^{-/-}$ mice.

Introduction

The tight regulation of Ca^{2+} is crucial for cochlear sensory cells. In response to sound stimulation, Ca^{2+} influx and Ca^{2+}-induced Ca^{2+} release (CICR) from the endoplasmic reticulum significantly increase intracellular Ca^{2+} in cochlear sensory cells. Factors that cause hearing impairment, such as ototoxic drugs, acoustic overstimulation, and aging, are associated with dysregulation of Ca^{2+} homeostasis (Fridberger & Ulfendahl, 1996; Kidd Iii & Bao, 2012; Liu & Fechter, 1997; Richard et al., 2023). Two types of specialized sensory cells in the mammalian cochlea, inner hair cells (IHCs) and outer hair cells (OHCs), are involved in the transduction of sound into electrical responses (Dallos, 1992). The OHCs are largely responsible for the sensitivity and tuning, whereas the IHCs transmit auditory signals to the brain via the auditory nerve. One of the hallmarks of cochlear injury following noise exposure is loss of OHCs. However, comparatively little is known about the endogenous mechanisms necessary to protect OHCs from the damaging effects of noise exposure. Intracellular Ca^{2+} concentration is significantly increased in auditory hair cells, especially OHCs, shortly after acoustic overstimulation (Fridberger et al., 1998; Zuo et al., 2008), and rapid increases in Ca^{2+} after noise exposure lead to hair cell loss (Esterberg et al., 2013; Fridberger et al., 1998; Orrenius et al., 2003). Thus, effective regulation of Ca^{2+} is essential for the responses of OHCs to noise.

Although evidence strongly suggests that Ca^{2+} overload can trigger apoptotic or necrotic cell death, and thus contribute to noise-induced damage, molecular models for Ca^{2+} overload are lacking. In OHCs, Ca^{2+} homeostasis depends upon the balance of Ca^{2+} influx, extrusion, and buffering. Oncomodulin (OCM) is a small, 12-kDa, EF-hand calcium-binding protein (CaBP) that is predominantly expressed in OHCs and functions differently from other EF-hand CaBPs (Climer et al., 2019; Murtha et al., 2022; Pangrsic et al., 2015). OCM is the β isoform of parvalbumin and shares at least 53% sequence identity with α-parvalbumin (PVALB). In adult mice, targeted deletion of OCM (*Ocm*$^{-/-}$) is the only EF-hand CaBP in OHCs associated with hearing loss to date. *Ocm*$^{-/-}$ mice have shorter hearing spans, independent of genetic background, which indicates the importance of OCM in the long-term maintenance of OHC function (Climer et al., 2021; Tong et al., 2016).

Recent studies show that the absence of OCM increases Ca^{2+} signaling in developing OHCs, and reveal that OCM plays a significant role in the synchronization of Ca^{2+} activity during cochlear maturation (Murtha et al., 2022; Yang Yang et al., 2023). In Murtha, Yang, et al (2022), we found that the onset of OCM expression alters the level of Ca^{2+} signals in OHCs before hearing onset. While there were changes in the expression of other CaBPs in response to the loss of OCM, these changes did not compensate for the loss of OCM function. These results support the idea that OCM plays a unique and indispensable role as a Ca^{2+} buffer in developing OHCs. Our previous findings also revealed higher levels of spontaneous Ca^{2+} activity, upregulation of purinergic receptors in OHCs, and higher synchronization of Ca^{2+} activity in *Ocm*$^{-/-}$ mice compared to wild-type mice (Yang et al. 2023). Additionally, the maturation of afferent synaptic ribbons in *Ocm*$^{-/-}$ OHCs was delayed, leading to an increased number of ribbon synapses and afferent fibers on OHCs before hearing onset. Given that OCM can modulate Ca^{2+} signaling and synchronization in OHCs during the pre-hearing period, and is essential for maintaining hearing in young adults, we hypothesize that the lack of OCM in adult mice disrupts Ca^{2+} homeostasis, increasing OHC vulnerability to noise.

In the present study, we used young adult *Ocm* knockout (*Ocm*$^{-/-}$) and age-matched controlsto study biophysical and electromotile responses as well as susceptibility to permanent hearing threshold shifts. Although *Ocm*$^{-/-}$ OHCs exhibited normal biophysical properties and electromotile responses, *Ocm*$^{-/-}$ mice showed a higher susceptibility to acoustic overstimulation with larger threshold shifts. Without noise stimulation, adult OHCs in *Ocm*$^{-/-}$ mice had higher purinergic P2X2 receptor expression and larger Ca^{2+} response induced by extracellular ATP. However, in response to noise exposure, P2X2 expression increased in the OHCs from *Ocm*$^{+/+}$, but not in *Ocm*$^{-/-}$ cochlea. Thus, we conclude that the increased vulnerability to noise in *Ocm*$^{-/-}$ mice may be associated with higher levels of both Ca^{2+} signaling and purinergic receptor expression, and ultimately leads to an early onset of age-related hearing loss.

Materials and Methods

Ethical approval

All procedures performed in the USA were approved by Baylor University and Mass Eye and Ear Institutional Animal Care and Use Committees (IACUC) as established by the US Public Health Service and performed in compliance with the National Institutes of Health animal care guidelines. Procedures performed in the UK and licensed by the Home Office under the Animals (Scientific Procedures) Act 1986 were approved by the University of Sheffield Ethical Review Committee.

Animals

Animals were bred in animal facilities at Baylor University, Mass Eye and Ear, and the University of Sheffield. The original *Ocm* mutant mouse (C57Bl/6 ActbCre; Ocmflox/flox) (Tong et al., 2016) was backcrossed onto the CBA/CaJ and the CBA/CaH background to minimize or eliminate any confounding effects of Cdh23ahl mutation, which is linked to hearing loss in the adult (Climer et al., 2021; Liu et al., 2007; Murtha et al., 2022). Studies using CBA/CaH mice were performed at the University of Sheffield, where mice were sacrificed via cervical dislocation in accordance with UK Home Office regulations.

We also generated mice with a genetically encoded, tissue-specific Ca^{2+} sensor (*Atoh1*-GCaMP6s) in *Ocm* wild-type (GCaMP6s-$Ocm^{+/+}$) and *Ocm* knockout (GCaMPs-$Ocm^{-/-}$) mice (Yang Yang et al., 2023). We first crossed *Ocm* wild-type ($Ocm^{+/+}$) and *Ocm* knockout ($Ocm^{-/-}$) mice with B6;129S-$Gt(ROSA)26Sor^{tm96.1(CAG\text{-}GCaMP6s)Hze}$/J, Ai96(RCL-GCaMP6s) or Ai96, which contains a floxed-STOP cassette preventing transcription of the GCaMP6 slow variant Ca^{2+} indicator. These mice were then crossed with knock-in transgenic mice expressing Cre recombined from the *Atoh1* locus (Chen et al., 2013). *Atoh1*-driven Cre GCaMP6s mice showed tissue-specific expression of endogenous green fluorescence (Cox et al., 2012; Mulvaney & Dabdoub, 2012; Yang et al., 2010).

Single-cell electrophysiology

For electrophysiological recordings, OHCs from CBA/CaH control ($Ocm^{+/-}$) and *Ocm*-knockout ($Ocm^{-/-}$) mice of both sexes were acutely dissected at 1 - 2 months. Cochleae were isolated from the inner ear as previously reported (Ceriani et al., 2019; Jeng et al., 2021; Jing-Yi Jeng et al., 2020; Marcotti & Kros, 1999; Murtha et al., 2022) using an extracellular solution composed of (in mM): 135 NaCl, 5.8 KCl, 1.3 $CaCl_2$, 0.9 $MgCl_2$, 0.7 NaH_2PO_4, 5.6 D-glucose, 10 HEPES-NaOH. Sodium pyruvate (2 mM), amino acids, and vitamins (Thermo Fisher Scientific, UK). The pH was adjusted to 7.5 (osmolality ~308 mmol kg^{-1}). The dissected cochleae were fixed at the bottom of the recording chamber by a nylon-meshed silver ring and perfused with the above extracellular solution. OHCs were viewed using an upright microscope (Olympus BX51) equipped with Nomarski Differential Interface Contrast (DIC) optics with a 60x water immersion objective and 15x eyepieces.

Recordings were performed at room temperature (21-24°C) using an Optopatch amplifier (Cairn Research Ltd, UK). Patch pipettes were pulled from soda glass capillaries and the shank of the electrode was coated with surf wax (2–3 MΩ). Current and voltage responses were measured using the following intracellular solution (in mM): 145 KCl, 3 $MgCl_2$, 1 EGTA-KOH, 5 Na_2ATP, 5 HEPES-KOH, 10 sodium phosphocreatine (pH adjusted to 7.28 with KOH; osmolality was 294 mmol kg^{-1}). Voltage clamp protocols were performed at a holding potential of −84 mV. Data acquisition was performed using pClamp software (Axon Instruments, Union City, CA, USA) using Digidata. Data were filtered at 2.5 kHz (8-pole Bessel), sampled at 5 kHz, and stored on the computer. Offline data analysis was performed using Origin software (OriginLab, Northampton, MA, USA). Membrane potentials reported were corrected for the uncompensated residual series resistance (R_s) and the liquid junction potential (LJP), which was 4 mV, measured between electrode and bath solutions.

Electromotile response:

Electromotility was estimated in OHCs at room temperature (~22°C) by applying a depolarizing voltage step from the holding potential of -64 mV to +56 mV and recorded using a CCD camera (Thorlabs DCU224M). The camera was attached to a microscope (Olympus), equipped with a X60 water immersion objective (Olympus LUMPlanFL N). The acquired images were stack-sliced along a vertical axis of each OHC and the contraction was measured on the image stack as length change of the cell. All images were analyzed in ImageJ and the measurements were calibrated using a stage graticule.

Noise exposure

Two different experimental approaches were used to assess the effects of noise exposure. The first approach assessed permanent threshold shifts, while the second approach assessed the immediate effects of chronic noise exposure. 4 - 6 wks old *Ocm*$^{+/+}$ and *Ocm*$^{-/-}$ CBA/CaJ mice and 3 - 4 wks old GCaMP6s - *Ocm*$^{+/+}$ and - *Ocm*$^{-/-}$ were randomly assigned to either noise-exposed or control groups. Cochlear thresholds of age-matched mice were measured 24 hrs prior to noise exposure. Controls were unexposed. For CBA mice, 2 hrs noise exposure were conducted, cochlear function was assessed 6 hrs following noise exposure and at 2 wks after noise exposure, followed by cochlear fixation and tissue harvest. For GCaMP6s mice, prolonged 9 hrs noise exposure were performed, cochlear function was assessed 1 hr following noise exposure followed by tissue harvesting.

For both groups, awake and unrestrained mice were placed in individual sections of a wire-mesh cage and exposed to either octave band noise (8-16 kHz, fifth-order Butterworth filter) for 2 hrs at 95.0 dB SPL, or broadband noise (centered at 2 kHz, with 8000, 3dB points bands width) for 9 hrs at 94.6 dB SPL. The booth is equipped with a JBL2446H compression driver coupled to an exponential horn. Noise levels were calibrated and monitored either with a 1⁄4″ Brüel and Kjær condenser microphone or a sound-level meter. The noise level varied by less than 2 dB over the duration of the exposures. Food and water were provided in a petri dish during 9 hrs of noise exposure.

Cochlear Function Assays

For measurement of distortion product otoacoustic emissions (DPOAEs), adult mice were anesthetized with xylazine (20 mg/kg, i.p.) and ketamine (100 mg/kg, i.p.). Acoustic stimuli were delivered using a custom acoustic assembly (Maison et al., 2012). Briefly, two electrostatic earphones (EC-1, Tucker Davis Technologies) were used to generate primary tones and a Knowles miniature microphone (EK-3103) was used to record ear-canal sound pressure. Stimuli were generated digitally with 4 s sampling. Ear-canal sound pressure and electrode voltage were amplified and digitally sampled at 20s for analysis of response amplitudes. The acoustic stimuli and physiological responses were digitized by a National Instruments PXI system with 24 - bit sound cards running custom LabVIEW software. ABRs were recorded via 30-gauge platinum electrodes, inserted subdermally, adjacent to the pinna incision and at the vertex of the skull, with a ground near the tail. Tone-pip stimuli were presented at half-octave frequency intervals from 5.6 - 45.2 kHz. At each frequency, a level series was presented, in 10 dB steps, from below threshold to 80 dB SPL, with up to 1024 stimuli averaged per step. Sound-evoked responses were amplified 10,000x through a 0.3 - 3 kHz bandpass filter. ABR threshold was defined as the lowest stimulus level to generate a waveform that increased in amplitude and decreased in latency as the stimulus level increased. For measurement of DPOAEs at 2f1 - f2, the primary tones were set so that the frequency ratio, (f2/f1), was 1.2 and so that f2 level was 10 dB below f1 level. For each f2/f1 primary pair, levels were swept in 10 dB steps from 20 dB SPL to 80 dB SPL (for f2). At each level, both waveform and spectral averaging were used to increase the signal-to-noise ratio of the recorded ear-canal sound pressure, and the amplitude of the DPOAE at 2f1 - f2 was extracted from the averaged spectra, along with the noise floor at nearby points in the spectrum. Iso-response curves were interpolated from plots of DPOAE amplitude vs. sound level. The threshold was defined as the f2 level required to produce a DPOAE at 0 dB SPL. Right ears were used for all hearing tests. For the total threshold shift of ABR and DPOAE, the total threshold shifts across all frequencies for each animal were calculated and then averaged across all animals.

Tissue preparation

Cochleae were harvested from 3 - 4 wks old *Ocm*$^{+/+}$ or *Ocm*$^{-/-}$ mice of either sex. After decapitation, apical coil OHCs were dissected from the organ of Corti in an extracellular medium composed of (in mM): 136.8 NaCl, 5.4 KCl, 0.4 KH_2PO_4, 0.3 Na_2HPO_4, 0.8 $MgSO_4$, 1.3 $CaCl_2$, 4.2 $NaHCO_3$, 5 HEPES and 5.6 glucose. The pH was adjusted to 7.4 - 7.5 (osmolality ~306 mmol/kg). The apical coil was then transferred to a small microscope chamber with nylon mesh fixed to a stainless-steel ring on the bottom and visualized using an upright microscope (Leica, DM 6000 FS, Germany) with a water immersion objective (Leica, Germany).

Confocal Ca^{2+} imaging

Ca^{2+} signals from GCaMP6s were recorded at room temperature with 480nm excitation wavelength (X-Light V2 spinning disk confocal, 89 North Inc, PRIME95B Photometrics Cooled sCMOS with 95% QE, Teledyne Photometric). Images were taken using VisiView (VISITRON, USA) and analyzed offline using ImageJ (NIH). Ca^{2+} signals were measured as relative changes in fluorescence emission intensity (ΔF/F0) and calculated by MATLAB. $\Delta F = F - F_0$, where F is fluorescence at time t and F0 is the fluorescence at the onset of the recording.

For inducing Ca^{2+} transients, the perfusion system started 8 s after the imaging started, 100 µl of ATP depolarization solution was added into a microscope chamber containing 300 µl extracellular solution (1:4 dilution, 100 µM ATP final concentration in the chamber), followed by a 2 min perfusion with the extracellular solution to help with equilibration. Only the fluorescence signals from OHCs that reached maximum intensity between 8-60 s were calculated. For the P2X antagonist experiments, the blocker, PPADS (100 µM), was added to the explant right before ATP application. Each GCaMP6s fluorescence recording includes 1500 frames taken at 80 frames per second from 1200 ×1200 pixels region. After background subtraction, the time course of Ca^{2+} changes in activated OHCs was computed as pixel averages of a circle region of interest (ROI) using ImageJ.

To assess the viability of these mature OHCs, we applied either a trypan blue solution (TB, final concentration 0.04%) or propidium iodide (PI, 500µM final concentration) immediately following (2 min) ATP treatment (3 min incubation for TB, or 5 min incubation for PI). Most OHCs were not permeable to TB after 3 mins of incubation and TB permeable cells were confined to the edges of cochlear spirals. No PI fluorescence could be detected after 5 mins of incubation. Finally, we induced cell death by adding saturated KCl, and strong red fluorescence was observed immediately after adding the high osmolarity solution. The addition of KCl also caused abnormal OHC shapes.

Genotyping and qRT-PCR

DNA was extracted from mice tail samples using Extract-N-Amp™ Tissue PCR Kit (Sigma, USA). PCR primers used for genotyping are listed below: *Atoh1*-Cre primer pair forward: 5’-CCGGCAGAGTTTACAGAAGC-3’, reverse: 5’-ATG TTT AGC TGG CCC AAA TG-3’; Cre control primer pair forward: 5’-CTA GGC CAC AGA ATT GAA AGA TCT-3’; reverse: 5’-GTA GGT GGA AAT TCT AGC ATC ATC C-3’; GCaMP6s primer pair forward: 5’- ACG AGT CGG ATC TCC CTT TG - 3’; reverse: 5’- AGA CTG CCT TGG GAA AAG CG - 3’; *Ocm* primer pair forward: 5’- CTC CAC ACT TCA CCA AGC AG - 3’, reverse: 5’- TTT CAT GTT CAG GGA TCA AGT G - 3’; *Ocm* deletion primer pair forward: 5’- CTC CAC ACT TCA CCA AGC AG - 3’, reverse: 5’- GCT TGG GGA CCC CCT GTC TTC A - 3’.

Cochleae were acutely dissected after anesthesia and transferred to the lysis buffer. Total RNA was extracted using RNeasy plus Micro kits (QIAGEN, USA). iScript™ Advanced cDNA Synthesis Kit (BIO-RAD, USA) was used for reverse transcription.

qRT-PCR was performed using the SYBR Green PCR Master Mix Kit (BIO-RAD, USA) as previously described (Murtha et al., 2022). Briefly, the *b2m* gene was used as a reference gene

(Melgar-Rojas et al., 2015). Quantification of expression (fold change) from the Cq data was calculated following the ΔΔCq method (Schmittgen & Livak, 2008), and normalized to the Cq value of *Ocm*$^{+/+}$. $2^{-\Delta\Delta Cq}$ was calculated to represent the relative expression (fold change). Primers used for qRT-PCR are as follows: *b2m* forward 5'-TGGTCTTTCTGGTGCTTGTC-3' and reverse 5'-GGG TGG AAC TGT GTT ACG TAG-3'; *P2RX2* forward 5'- GCG TTC TGG GAC TAC GAG AC -3' and reverse 5'- ACG TAC CAC ACG AAG TAA AGC -3' (PrimerBank ID 27544798a1).

Immunofluorescence microscopy

Histological analysis and immunocytochemistry were performed (Climer et al., 2021) (Murtha et al., 2022). Briefly, cochleae were flushed with 4% PFA and then fixative overnight at 4°C with rotation. Cochleae were then decalcified in 0.1M EDTA for 3 - 5 days at 4°C with rotation. The apical coils of cochleae were then dissected or prepared as 100 µm mid-modiolar sections embedded in the gelatin-agarose solution (Maison et al., 2012; Simmons et al., 2010). Microdissected cochlear pieces were suspended in 30% sucrose for 30 - 60 min at room temperature with gentle shaking, frozen at -80°C for 30 min, then thawed for 30 min at 37°C. Pieces were washed 3 times in PBS, then blocked in 5% normal horse serum (NHS) for 1 hr at room temperature. Samples were stained with antibodies to P2X2 (Alomone Labs, Israel, APR-003, 1:400). Primary antibodies were incubated overnight at 37ºC. Appropriate Northern Lights (R&D Systems 1:200) conjugated secondary antibodies were incubated for 1 hr at 37ºC. Slides were prepared using Vectashield mounting media with DAPI (Vector Laboratories, USA). Images were acquired using the LSM800 microscope using a high-resolution, oil-immersion objective (Zeiss, Germany). Cohorts of samples were immunostained at the same time and imaged under the same optical conditions to allow for direct comparison.

Western Blotting

Cochleae were dissected and harvested in ice-cold PBS. Cochleae were then transferred into a pre-cooled tube (one cochlea per sample) containing 250 µL ice-cold RIPA-lysis buffer containing: 1% Triton X-100, 25 mM Tris, pH 7.4, 150 mM NaCl, 1 mm DTT, 1 mm $MgCl_2$, 1 mM phenylmethylsulfonyl fluoride, and 1x protease inhibitor cocktail (Thermo Scientific). A hand-on homogenizer (Kimble Pellet Pestle, DWK Life Science) was used to crack up cochleae manually, followed by an additional 30 min incubation in lysis buffer. Cochlear lysates were further sonicated (Fisher Scientific) 3 times x 5 seconds each on ice. Samples were then transferred to a rotating wheel at 4°C for an additional 60 min, lysates were spun down at 4°C, 12000 x g for 5 min to remove cell debris. The supernatants were then transferred to a new tube and heated for 30 minutes at 37°C in 4X SDS-sample buffer (BIO-RAD, 355 mM β-ME added). Samples were then subject to SDS-PAGE and protein was transferred to a PVDF membrane. Membranes were blocked with 2.5% fish gelatin for 1 hr at RT and incubated overnight at 4°C with primary antibody to rabbit P2X2R (1:400, Alomone Labs) and rabbit β-tubulin (1:1000). After washing, membranes were incubated with appropriate HRP-conjugated secondaries (anti-rabbit 1:7,500) for 1 hr at RT. Clarity Max ECL Substrate (BIO-Rad, USA) was used to detect chemiluminescence via a ChemiDoc imaging system. Relative protein expression levels (normalized to β-tubulin) were determined by densitometric analysis using FIJI software.

Statistical analysis

Statistical analysis was performed using GraphPad Prism 9 and MATLAB software. Statistical comparisons of means were made by t-test or, when normal distribution could not be assumed, the Mann-Whitney U-test. For multiple comparisons, one-way or two-way ANOVA followed by Bonferroni post-test was used unless otherwise stated. Data is given as mean ± SD. Animals of either sex were randomly assigned to the different experimental groups. No statistical methods were used to define the sample size, which was selected based on previously published similar work from our laboratories. Animals were taken from multiple cages and breeding pairs.

Results

OHCs from Ocm$^{-/-}$ mice exhibited normal biophysical profiles

At postnatal day 3 (P3), OHCs from *Ocm*$^{-/-}$ mice exhibit normal biophysical profiles (Murtha et al., 2022). Therefore, we investigated whether the lack of OCM had any effect on mature OHC biophysical profiles and electromotility. In 1-2-month-old (mo) CBA/CaH mice, we examined the potassium currents in OHCs while applying a series of hyperpolarizing and depolarizing voltage steps from the holding potential of -84mV with 10 mV increments (**Figure 1A, B**). The time course and voltage dependence of the outward K^+ currents in OHCs were comparable between *Ocm*$^{-/-}$ and control OHCs (**Figure 1A-C**). We then tested OHC electromotile responses. In line with normal morphological appearance, OHCs from *Ocm*$^{-/-}$ mice showed normal electromotile activity at 1-2 mo. Under whole-cell patch clamp conditions, stepping the membrane potential from −84 mV to +40 mV caused OHCs to shorten, as previously described (J. Y. Jeng et al., 2020; Marcotti & Kros, 1999). OHC contraction was not significantly different between the two genotypes (**Figure 1D, E**). Similar to immature OHCs, lack of OCM does not affect OHC electrophysiology in young adult mice.

Lack of OCM increases permanent threshold shifts after 2-hr noise exposure

Young mice have a heightened vulnerability to noise during a sensitive period between 1 mo to 4 mo (Kujawa & Liberman, 2006; Ohlemiller et al., 2010; Ohlemiller & Gagnon, 2007). We investigated whether the absence of OCM increases vulnerability to moderate levels of noise exposure that are associated with temporary threshold shifts (TTS) using octave band noise (8 - 16 kHz, 95.0 dB SPL, 2 hrs, **Figure 2A**) (Kujawa & Liberman, 2009). We used 95 dB SPL for 2 hrs to cause maximum TTS with minimal or no permanent threshold shift (PTS) in CBA/CaJ mice (Fernandez et al., 2010; Hirose & Liberman, 2003). Pre-exposure (24 hrs before) and post-exposure (6 hrs and 14 days) ABR testing was performed at three frequencies (8, 16, and 32 kHz) and DPOAE testing at seven frequencies (5.66, 8.00, 11.32, 16.00, 22.56, 32.00, and 45.20 kHz). As shown in **Figure 2B-C**, noise exposure altered ABR thresholds in both *Ocm*$^{+/+}$ and *Ocm*$^{-/-}$ mice ($p < 0.01$ for *Ocm*$^{+/+}$ and *Ocm*$^{-/-}$ mice, *two-way ANOVA*). At 6 hrs after noise exposure, ABR thresholds at 32 kHz showed a significant increase in *Ocm*$^{+/+}$ mice ($p < 0.0001$, *Bonferroni* post-test, **Figure 2C**), while all three tested frequency regions in *Ocm*$^{-/-}$ mice were significantly increased ($p < 0.01$ for 8 kHz, $p < 0.05$ for 16 and 32kHz, **Figure 2C**). ABR threshold shifts at 16 kHz were comparable between *Ocm*$^{+/+}$ and *Ocm*$^{-/-}$ mice 6 hrs after noise exposure. However, after 2 wks of recovery, *Ocm*$^{-/-}$ mice showed a significantly higher ABR threshold shift at 16 kHz compared to *Ocm*$^{+/+}$ mice ($p < 0.05$, **Figure 2D**).

As shown in **Figure 3A**, DPOAEs thresholds were also significantly increased in both *Ocm*$^{+/+}$ and *Ocm*$^{-/-}$ mice 6 hrs after noise exposure ($p < 0.0001$ for *Ocm*$^{+/+}$ and *Ocm*$^{-/-}$ mice, *two-way ANOVA*, **Figure 3A).***)*. Specifically, *Ocm*$^{+/+}$ mice showed significantly increased DPOAE thresholds at 16 kHz ($p < 0.01$, *Bonferroni* post-test), 22 and 32 kHz ($p < 0.0001$, *Bonferroni* post-test), while *Ocm*$^{-/-}$ mice showed significantly higher DPOAE thresholds at 8 kHz ($p < 0.05$, *Bonferroni* post-test), 16 and 22 kHz ($p < 0.0001$, *Bonferroni* post-test) 6 hrs after noise exposure. After 2 wks, DPOAE thresholds from *Ocm*$^{+/+}$ mice mostly recovered from noise exposure, with the exception of the 32 kHz region compared to pre-noise ($p < 0.01$, *Bonferroni* post-test). However, *Ocm*$^{-/-}$ mice still exhibited higher DPOAE thresholds in mid to high-frequency regions (16 and 22 kHz, $p < 0.01$, 32 and 45 kHz, $P < 0.05$). We then compared DPOAE input-output functions at 16 kHz in *Ocm*$^{+/+}$ and *Ocm*$^{-/-}$ mice before and after noise exposure (**Figure 3B**). At 6 hrs post-noise exposure, both *Ocm*$^{+/+}$ and *Ocm*$^{-/-}$ mice required stronger stimuli (~10dB SPL) to produce DPOAE outputs that crossed the threshold criterion (0 dB). However, 2 wks after noise exposure, *Ocm*$^{-/-}$ mice showed lower suprathreshold DPOAE amplitudes, while *Ocm*$^{+/+}$ mice recovered to pre-noise input levels (dB SPL) **Figure 3B**). The mean total DPOAE threshold shifts across all frequencies, 6 hrs after noise exposure were comparable between *Ocm*$^{+/+}$ and *Ocm*$^{-/-}$ mice (**Figure 3C**). However, 2 wks after noise exposure, *Ocm*$^{-/-}$ mice showed larger DPOAE threshold shifts than *Ocm*$^{+/+}$ mice ($p < 0.05$. *two-way ANOVA*, **Figure 3C**). The faster recovery from noise exposure in *Ocm*$^{+/+}$ mice suggests that OCM may be involved in protecting protecting mice from PTS, at least, after moderate noise exposures.

Lack of OCM increases threshold shifts after 9-hr noise exposure

Similar to noise exposure (Zuo et al., 2008), loss of OCM causes increased levels of intracellular free Ca^{2+} (Murtha et al., 2022). We hypothesized that the early progressive hearing loss observed in *Ocm*$^{-/-}$ mice is partly due to prolonged Ca^{2+} overload in *Ocm*$^{-/-}$ OHCs. To investigate Ca^{2+} activity in adult *Ocm*$^{-/-}$ mice, we expressed a genetically encoded, tissue-specific Ca^{2+} sensor (*Atoh1*-GCaMP6s) in *Ocm*$^{+/+}$ and *Ocm*$^{-/-}$ mice as previously described (Yang Yang et al., 2023). We first compared the differences in susceptibility to prolonged (9-hr) at 3 - 4 wks of age. DPOAE and ABR thresholds were measured 48 hrs before noise stimulation, followed by 9 hrs of continuous broadband noise stimulation at 95 dB SPL to mimic chronic noise exposure. Post-noise DPOAEs and ABRs were measured immediately after exposure (**Figure 4A**). ABR thresholds at 16 kHz were significantly elevated in both *Ocm*$^{+/+}$ and *Ocm*$^{-/-}$ mice after noise stimulation ($p < 0.01$ for *Ocm*$^{+/+}$ and *Ocm*$^{-/-}$, *t*-test, **Figure 4B**). Further, *Ocm*$^{-/-}$ mice showed a higher total ABR threshold shift compared to *Ocm*$^{+/+}$ mice ($p < 0.05$, *t*-test, **Figure 4C**). In *Ocm*$^{+/+}$ mice, we observed significantly increased DPOAE thresholds only at 22 kHz ($p < 0.01$, *Bonferroni* post-test, **Figure 4D**). However, in *Ocm*$^{-/-}$ mice, we found significant differences in DPOAE thresholds after noise exposure at 11, 16 ($p < 0.0001$), and 22 kHz frequencies ($p < 0.001$, **Figure 4D**). The average DPOAE threshold shift throughout all frequencies in *Ocm*$^{-/-}$ mice was significantly higher compared to *Ocm*$^{+/+}$ mice ($P < 0.05$, *t*-test, **Figure 4E**). Using the same experimental timeline but without noise stimulation (control), we found no significant difference in DPOAEs and ABR thresholds between the 1st and 2nd measurements (**Figure 4F-G**). The above data indicate that compared to *Ocm*$^{+/+}$ mice, *Ocm*$^{-/-}$ mice have increased susceptibility to prolonged noise.

ATP-induced Ca^{2+} transients in mature OHCs are higher in Ocm$^{-/-}$ mice and after prolonged noise exposure

We investigated whether the higher susceptibility of *Ocm*$^{-/-}$ mice to noise exposure was a result of increased Ca^{2+} signaling in OHCs, as previously found in pre-hearing mice (Murtha et al., 2022; Yang et al., 2023). Apical cochleae from 3 - 4 wks old *Ocm*$^{+/+}$ and *Ocm*$^{-/-}$ GCaMP6s mice were dissected (**Figure 5A**) and immediately transferred to the microscope chamber. ATP (100 μM) was extracellularly applied to induce Ca^{2+} transients (**Figure 5B**), which were measured as fractional changes of GCaMP6s fluorescence ($\Delta F/F_0$) (**Figure 5C** gray line). *Ocm*$^{-/-}$ OHCs showed significantly larger ATP-induced Ca^{2+} transients compared to *Ocm*$^{+/+}$ OHCs ($p < 0.001$, *two-way ANOVA*, **Figure 5D**). We also found that prolonged noise stimulation (**Figure 4**) caused a significantly increased maximum $\Delta F/F_0$ in OHCs from both *Ocm*$^{+/+}$ and *Ocm*$^{-/-}$ mice after 9 hrs of noise exposure ($p < 0.001$, *two-way ANOVA*, **Figure 5D**). Post-noise OHCs from *Ocm*$^{-/-}$ mice exhibited a higher maximum $\Delta F/F_0$ signal compared to littermate *Ocm*$^{+/+}$ OHCs ($p < 0.001$, *Bonferroni* post-test, **Figure 6D**). Further, maximum $\Delta F/F_0$ signals were comparable between pre-noise *Ocm*$^{-/-}$ OHCs and post-noise *Ocm*$^{+/+}$ OHCs (**Figure 5D**).

To test whether the ATP and noise-induced Ca^{2+} responses in OHCs were caused by purinergic receptors, we used the non-selective purinergic receptor antagonist PPADS (100 μM). Extracellular application of PPADS nearly abolished ATP-induced Ca^{2+} transients in OHCs and eliminated the significant difference in the maximum $\Delta F/F_0$ between *Ocm*$^{+/+}$ and *Ocm*$^{-/-}$ before and after noise exposure **(Figure 5E)**. These data indicate that the lack of OCM increases ATP-induced Ca^{2+} transients in mature OHCs, which mimic the effects caused by long-term noise exposure.

The lack of OCM and prolonged noise stimulation up-regulated P2X2 receptors

We tested whether the larger Ca^{2+} responses in adult *Ocm*$^{-/-}$ mice were due to the increased expression of P2X2 receptors, which have been shown to be up-regulated during prehearing stages (Y. Yang et al., 2023). Without noise exposure, the expression of *P2RX2* in the cochlea of 3-4wks *Ocm*$^{-/-}$ mice was significantly higher than that in *Ocm*$^{+/+}$ mice ($p < 0.01$, *Bonferroni* post-test, **Figure 6A**). After prolonged noise exposure, *P2RX2* expression was upregulated in the *Ocm*$^{+/+}$ cochlea ($p < 0.01$, *Bonferroni* post-test) but not in *Ocm*$^{-/-}$ mice (**Figure 6A**). Furthermore, there was no significant difference in *P2RX2* expression between post-noise *Ocm*$^{+/+}$ and *Ocm*$^{-/-}$ OHCs (**Figure 6A**). Using immunostaining from We also examined P2X2 receptor localization in the mature pre-noise organ of Corti. Using mid-modiolar sections, we found that P2X2 receptors localize on the surface of the organ of Corti (facing the scala media) in both *Ocm*$^{+/+}$ and *Ocm*$^{-/-}$ mice (**Figure 6B**). Before noise exposure, *Ocm*$^{-/-}$ but not *Ocm*$^{+/+}$ mice showed stronger P2X2 receptor labeling in OHCs, especially near the cuticular plate (**Figure 6B,** red arrow). In apical spirals, the expression of P2X2 receptors was compared between pre- and post-noise exposure. Before noise exposure, *Ocm*$^{-/-}$ mice showed stronger P2X2 receptor labeling compared to *Ocm*$^{+/+}$ mice (**Figure 6C**). After prolonged noise exposures, *Ocm*$^{+/+}$ OHCs showed upregulated P2X2 receptor immunolabeling compared to pre-noise *Ocm*$^{+/+}$ mice (**Figure 8C,** pointed with red arrow). There were no obvious changes between pre- and post-noise *Ocm*$^{-/-}$ OHCs. Western blot experiments revealed that prolonged noise stimulation significantly upregulated the expression of P2X2 receptors only in *Ocm*$^{+/+}$ mice ($p < 0.01$, *Bonferroni* post-test, **Figure 6E**) but not in *Ocm*$^{-/-}$ cochleae (**Figure 6E**). The expression of P2X2 receptor in pre-noise *Ocm*$^{-/-}$ mice showed no significant difference compared to post-noise *Ocm*$^{+/+}$ mice (**Figure 6E**). These results show that the lack of OCM led to an upregulation of *P2RX2* mRNA expression in the cochlea of *Ocm*$^{-/-}$ mice, which was not further increased after prolonged noise exposure.

Both the lack of OCM and the endogenous expression of GCaMP6s accelerate progressive hearing loss

The lack of OCM and prolonged noise exposure can lead to a Ca^{2+} dysregulation in hair cells, adversely affecting hearing. As a Ca^{2+} sensor, GCaMP6s contains a calmodulin domain might also disrupt the calcium homeostasis over time. Endogenous expression of GCaMP6s had little or no impact on auditory function at early adult ages. but did have a significant impact on auditory function at later adult ages. *Ocm*$^{+/+}$ and *Ocm*$^{-/-}$ mice with endogenous expression of GCaMP6s exhibited comparable DPOAE thresholds at 3 - 4 wks old (Yang Yang et al., 2023). Here, we investigated the long-term impact of GCaMP6s expression within the inner ear. By measuring DPOAEs, we investigated OHC function *in vivo* from both GCaMP6s negative (GCaMP6s-) or GCaMP6s positive (GCaMP6s+) *Ocm*$^{+/+}$ and *Ocm*$^{-/-}$ mice during aging. At 3 - 4 wks, neither the endogenous expression of GCaMP6s nor the absence of OCM affects DPOAE thresholds across all frequencies ($P = 0.69$ for *Ocm*$^{+/+}$ vs. *Ocm*$^{-/-}$, $P = 0.29$ for GCaMP6s- vs. GCaMP6s+. *three-way ANOVA*, **Figure 7A**). There were no significant differences at 16 kHz at this age among GCaMP6s- and GCaMP6s+, *Ocm*$^{+/+}$ and *Ocm*$^{-/-}$ mice ($P = 0.62$, *two-way ANOVA*, **Figure 7D**). At 12 - 13 wks and 20 - 22 wks, *Ocm*$^{-/-}$ mice exhibited increased DPOAE thresholds compared to *Ocm*$^{+/+}$ mice (**Figure 7B-C, E-F**), which is consistent with previous studies (Climer et al., 2021; Tong et al., 2016). Further, the endogenous expression of GCaMP6s accelerated progressive hearing loss ($P < 0.0001$ for *Ocm*$^{+/+}$ vs. *Ocm*$^{-/-}$, and for GCaMP6s- vs. GCaMP6s+. *three-way ANOVA*, **Figure 7B-C**). At 20-22 wks, all GCaMP6s+ mice, including *Ocm*$^{+/+}$ and *Ocm*$^{-/-}$ mice, were essentially deaf (**Figure 7C, F**). These data indicate that the expression of GCaMP6s also has deleterious consequences in hearing, and accelerates progressive hearing loss.

Discussion

In the present study, we show that OHCs lacking the buffering protein OCM, have increased vulnerability to noise exposure and higher expression of purinergic receptors at young adult ages. We first performed 2 hrs noise exposure, both *Ocm*$^{+/+}$ and *Ocm*$^{-/-}$ mice exhibit similar TTS 6 hrs post noise exposure, however *Ocm*$^{-/-}$ mice show PTS after 2 wks recovery. Using GCaMP6s mice (Yang Yang et al., 2023), we found prolonged noise exposures (95 dB SPL, 9 hrs) produced higher threshold shifts and increased ATP-induced Ca^{2+} signaling in *Ocm*$^{-/-}$ apical OHCs compared to littermate *Ocm*$^{+/+}$ controls. These prolonged noise exposures led to increased expression of purinergic P2X2 receptors in the cochlea of *Ocm*$^{+/+}$ but not in *Ocm*$^{-/-}$ mice. Upregulated ATP-induced Ca^{2+} responses and saturating levels of P2X2 indicate that mature *Ocm*$^{-/-}$ OHCs may have a higher Ca^{2+} load, as previously shown. In fact, we found previously that higher intracellular Ca^{2+} concentration in these mice at pre-hearing stages of development (Murtha et al., 2022). All these data confirm that OCM plays a key role in shaping Ca^{2+} dynamics in OHCs.

Our results further demonstrate the importance of OCM as a specialized Ca^{2+} buffer in OHCs. The homeostatic control of intracellular Ca^{2+} is likely to contribute to the sensitivity of the OHCs to cochlear injury (Mammano, 2011). Ca^{2+} signaling plays fundamental roles in cochlear development and function, including mechanotransduction, neurotransmitter release, innervation, and motility (Ceriani & Mammano, 2012). We recently demonstrated that *Ocm*$^{-/-}$ OHCs in the prehearing cochlea altered Ca^{2+} signaling and delayed maturation of innervation (Yang Yang et al., 2023). Aberrant Ca^{2+} in hair cells leads to cochlear pathology (Richard et al., 2023) and there is increased OHC loss in *Ocm*$^{-/-}$ mice (Climer et al., 2021; Tong et al., 2016). Noise exposure is a common cause of hearing loss, and increases the concentration of cytosolic free Ca^{2+} (Fridberger et al., 1998; Zuo et al., 2008). Ca^{2+} overload in sensory hair cells contributes significantly to hair cell apoptotic and necrotic pathways, which in turn, could exacerbate inflammatory responses (Bienkowski et al., 2000; Esterberg et al., 2013; Fridberger et al., 1998; Fu et al., 2021; Orrenius et al., 2003). Thus, tightly regulation of intracellular Ca^{2+} signaling through specialized mobile CaBPs such as OCM (Climer et al., 2019), is essential for OHC survival, especially after noise exposure.

Although the lack of OCM results in early-onset hearing loss, *Ocm*$^{-/-}$ mice have normal hearing thresholds at least through the first 3 - 4 wks of age (Climer et al., 2021; Tong et al., 2016). This period of normal hearing thresholds in the absence of OCM suggests that there may be alternative mechanisms at play that provide temporary regulation of intracellular Ca^{2+} signals and maintain OHC function. Homeostatic control of intracellular Ca^{2+} levels is a complex function of influx, efflux and buffering. We previously found that both Cav1.3 mRNA (*CACNA1D*), which serves as one of the main Ca^{2+} entry points in hair cells (Michna et al., 2003; Platzer et al., 2000), we investigated whether expression was altered in prehearing mice (Yang Yang et al., 2023). We previously found both Cav1.3 mRNA (*CACNA1D*) and protein expression in the cochlea of *Ocm*$^{-/-}$ mice was down-regulated compared to control mice (Yang Yang et al., 2023). We speculate that this downregulation might indeed be a response to prevent Ca^{2+} overloading in OHCs and thus protect them from cytotoxicity. A similar compensatory mechanism may also exist in young adult OHCs to temporarily maintain the uncompromised function of hearing.

Since OHC Ca^{2+} buffering is dominated by OCM (Hackney et al., 2005), in the absence of OCM, other mobile buffers such as calbindin-D28k or αPV might substitute for its absence. However, recent studies have shown changes in other mobile EF-hand CaBPs are not likely responsible for modulating intracellular Ca^{2+} levels (Murtha et al., 2022; Pangrsic et al., 2015; Yang Yang et al., 2023). In cochlear hair cells, mitochondria can also modulate intracellular Ca^{2+} homeostasis via the mitochondrial Ca^{2+} uniporter (MCU) and extruding Ca^{2+} back to the cytosol through the sodium-calcium exchanger (NCLX). MCU expression increased after noise exposure while the expression of NCLX decreased in a time- and exposure-dependent manner (Wang et al., 2018). Thus, OHC mitochondria could compensate for the absence of OCM and temporarily maintain the function of OHCs. However, long-term mitochondrial Ca^{2+} overload could also cause mitochondrial stress, induce OHC death, and subsequently hearing loss (Vicente-Torres & Schacht, 2006). This latter scenario might explain the early, progressive OHC loss observed in *Ocm*$^{-/-}$ mice.

Similar to our previous studies in prehearing mice (Yang Yang et al., 2023), we found that the expression of P2X2 purinergic receptors was upregulated in young adult *Ocm*$^{-/-}$ mice compared to control mice. The upregulation of purinergic receptors could be a compensatory mechanism for Ca^{2+} overload. In mature hair cells, P2X2 is a modulator of auditory sensory hair cell mechanotransduction, which plays an essential role in hair cell tolerance to noise (Mittal et al., 2016). In agreement with our study, noise exposure leads to an upregulation of *P2RX2* mRNA and protein levels in the organ of Corti (Telang et al., 2010; Wang et al., 2003). The high expression of purinergic receptors, with the increase of the local ATP release in the endolymph and perilymph (Munoz et al., 1995; Telang et al., 2010), provides a latent shunt capable of regulating the majority of electrical potential across the luminal surface of the sensory hair cells (Thorne et al., 2004), resulting in a longer-lasting sensitivity reduction. The mutation of *P2RX2* in both humans and mice gives rise to progressive hearing loss and increased sensitivity to permanent threshold shifts (Yan et al., 2013), which suggests that the P2X2 receptor modulates hearing adaptation and protects the cochlea from permanent damage. Furthermore, a recent study revealed an increased purinergic response in supporting cells from the aged cochlea (Hool et al., 2023), indicating a possible protective mechanism during aging that prevents further damage to the sensory epithelium. Indeed, $Ocm^{-/-}$ mice exhibit upregulation of P2X2 in the cochlea at both neonatal and young adult stages. However, since the purinergic signaling also contributes to inflammation and immune responses (Burnstock, 2016; Liu et al., 2023), the long-term overexpression of purinergic receptors in OHCs could also be toxic to normal hearing.

Taken together, OCM protects OHCs from acoustic overstimulation. The lack of OCM induces chronic Ca^{2+} dysregulation such as increased ATP-induced Ca^{2+} activity, and higher expression of ATP receptors in OHCs, which is associated with an increased susceptibility to noise. We propose that as a CaBP, OCM regulates Ca^{2+} signals in OHC and protects OHC from the deleterious consequences of Ca^{2+} overload.

Figure legends:

Figure 1. Biophysical properties of OHCs are not affected in early postnatal CBA/CaH *Ocm*$^{-/-}$ mice. K$^+$ currents from control OHCs **(A)** and *Ocm*$^{-/-}$ **(B)** 1 - 2 months age CBA/CaH mice. Recordings were performed by applying a series of voltage steps in 10 mV nominal increments from the holding potential of -84 mV. **(C)** Average current-voltage curves from control and *Ocm*$^{-/-}$ OHCs of 1-2 months, n = 4 for each genotype, mean ± SEM. **(D, E)** *Ocm*$^{-/-}$ OHCs showed a comparable contraction distance. n = 7, 21 control OHCs, n = 4, 12 *Ocm*$^{-/-}$ OHCs were measured, mean ± SD with single recordings in open circles, *t*-test.

Figure 2 *Ocm*$^{-/-}$ mice showed increased ABR threshold shifts after noise exposure. (A) Schematic of noise exposure experiment timeline using CBA/CaJ *Ocm*$^{+/+}$ or *Ocm*$^{-/-}$ mice at 1-2 months of age (mo). DPOAEs and ABRs were tested 24 hrs prior to the noise, followed by 2 hrs 95.0 dB SPL broadband noise exposure. DPOAEs were then measured 6 hrs after, and 2 wks after noise exposure. **(B)** Representative ABR waveforms at 16 kHz from CBA/CaJ *Ocm*$^{+/+}$ and *Ocm*$^{-/-}$ mice before 6 hrs after, and 2 wks after noise exposure. **(C)** ABR thresholds from 1-2 mo CBA/CaJ *Ocm*$^{+/+}$ (black/left) and *Ocm*$^{-/-}$ (red/right) mice at 8 kHz, 16 kHz, and 32 kHz before, 6 hrs after, and 2 wks after noise exposure. $n \geq 4$ for each genotype, mean ± SD, $p < 0.001$ for both *Ocm*$^{+/+}$ and *Ocm*$^{-/-}$ mice between pre-noise and 6 hrs post-noise, *two-way ANOVA*. Significance shown as asterisks (*) indicates significant differences between pre-noise and 6 hrs post noise, no significant differences between pre-noise and 2 wks post noise. **(D)** Average of ABR threshold shifts at 16 kHz, mean ± SD, $p < 0.05$, *two-way ANOVA*. *: $p < 0.05$, **: $p < 0.01$, ***: $p < 0.001$, *Bonferroni* post-test.

Figure 3 *Ocm*$^{-/-}$ mice showed increased DPOAE threshold shifts after noise exposure. (A) DPOAE thresholds from 1-2 mo CBA/CaJ *Ocm*$^{+/+}$ and *Ocm*$^{-/-}$ mice before, 6 hrs after, and 2 wks after noise exposure. $n \geq 7$ for each genotype. Mean ± SD, $p < 0.001$ for both *Ocm*$^{+/+}$ and *Ocm*$^{-/-}$ mice between pre-noise and 6 hrs post-noise, and *Ocm*$^{-/-}$ mice between pre-noise and 2 wks post-noise *two-way ANOVA*. Significance shown as asterisks (*) means the comparison between pre-noise and 6 hrs post-noise, and the number signs (#) represents the comparison between pre-noise and 2 wks post-noise. */#: $p < 0.05$, **/##: $p < 0.01$, ***: $p < 0.001$, *Bonferroni* post-test. **(B)** DPOAE input/output functions from CBA/CaJ *Ocm*$^{+/+}$ and *Ocm*$^{-/-}$ mice pre- and post-noise exposure, mean ± SD. **(C)** Average of total DPOAE threshold shifts from all frequencies, mean ± SD, $P < 0.05$, *two-way ANOVA*. *: $p < 0.05$, *Bonferroni* post-test.

Figure 4. *Ocm*$^{-/-}$ mice showed increased susceptibility after prolonged noise exposure. (A) Schematic of noise exposure experiment timeline using *Ocm*$^{+/+}$ or *Ocm*$^{-/-}$ mice with endogenous expression of GCaMP6s at 3 - 4 weeks (wks) of age. ABRs and DPOAEs were tested 48 hours (hrs) prior to the noise, followed by a 9 hrs 94.6 dB SPL broadband noise exposure. DPOAEs were then measured immediately after noise exposure. **(B)** Representative ABR threshold at 16 kHz from 3 - 4 wks old *Ocm*$^{+/+}$ and *Ocm*$^{-/-}$ mice before and after noise exposure. mean ± SD. **: $p < 0.01$, t-test. **(C)** Average of ABR threshold shifts at 16 kHz after noise exposure, n = 6 for each genotype, mean ± SD. **: $p < 0.01$, *t*-test. **(D)** DPOAEs from 3 - 4 wks old *Ocm*$^{+/+}$ and *Ocm*$^{-/-}$ mice before and after noise exposure. n = 6 for each genotype. $p < 0.01$ for *Ocm*$^{+/+}$ and *Ocm*$^{-/-}$ mice, *two-way ANOVA*. Significance shown as asterisks, *: $p < 0.05$, **: $p < 0.01$, ***: $p < 0.001$, *Bonferroni* post-test. **(E)** The average of total DPOAE threshold shifts was measured from all frequencies, mean ± SD. *: $p < 0.05$; *t*-test. **(F)** The control group showed no significant difference in DPOAE and ABR thresholds. 1st and 2nd DPOAEs and ABRs were tested 48 hrs prior to the noise, settled in a sound isolation room for extra 9 hrs, and were measured again simultaneously with the experiment group. Average of ABR threshold shifts at 16 kHz, n = 3 for each genotype, mean ± SD. ns: not significant, *t*-test. **(G)** DPOAE thresholds from 3 - 4 wks GCaMP6s *Ocm*$^{+/+}$ and *Ocm*$^{-/-}$ control mice (n = 3 for each genotype), *two-way ANOVA* followed by multiple comparisons. No significant difference shown at 5.66, 8, 11.32, 16, 22.56 and 45.2KHz region.

Figure 5 The absence of OCM alters ATP-induced Ca^{2+} transient in OHCs similar to noise. (A) Cochleae were taken from 3 - 4 wks old mice with endogenous expression of GCaMP6s. Apical cochlear spirals were immediately dissected and tested. The dashed box shows the region for the Ca^{2+} transient imaging. **(B)** Representative images from pre-noise *Ocm*$^{+/+}$ and *Ocm*$^{-/-}$ mice showing Ca^{2+} transients in OHCs induced by 100 μM extracellular ATP. GCaMP6s fluorescence before ATP superfusion (top), at peak response (middle), and recovery stage (bottom) are shown. **(C)** Representative traces of fluorescence fractional change ($\Delta F/F_0$) in OHCs from *Ocm*$^{+/+}$ and *Ocm*$^{-/-}$ OHCs pre- or post-noise exposure (light gray line), average $\Delta F/F_0$ shown as bold lines. **(D, E)** Maximum $\Delta F/F_0$ in OHCs from *Ocm*$^{+/+}$ and *Ocm*$^{-/-}$ mice pre- or post-noise exposure induced by 100 μM ATP, or with the presence of PPADS (100 μM). For the maximum $\Delta F/F_0$ of ATP-induced Ca^{2+} transients, $n \geq 4$ for each genotype under each treatment, 73 and 93 OHCs from pre-noise *Ocm*$^{+/+}$ and *Ocm*$^{-/-}$ mice, 83 and 49 OHCs from post-noise *Ocm*$^{+/+}$ and *Ocm*$^{-/-}$ mice were measured. $p < 0.001$, *two-way ANOVA*. For the PPADS experiment, n = 2 for each genotype under each treatment, 22 and 29 OHCs from pre-noise *Ocm*$^{+/+}$ and *Ocm*$^{-/-}$ mice, 15 and 13 OHCs from post-noise *Ocm*$^{+/+}$ and *Ocm*$^{-/-}$ mice were measured. *: $p < 0.05$; **: $p < 0.01$; ***: $p < 0.001$, *Bonferroni* post-test.

Figure 6 P2X purinoceptor 2 (P2X2) expression only upregulated in *Ocm*$^{+/+}$ mice after noise stimulation. (A) qRT-PCR results of *P2RX2* relative expression, cochleae are taken from 3 - 4 wks *Ocm*$^{+/+}$ and *Ocm*$^{-/-}$ mice with or without noise exposure. Total mRNA was extracted immediately after dissection. $n \geq 3$ for each genotype under each experimental condition. All values were normalized to pre-noise *Ocm*$^{+/+}$. mean ± SD, $p < 0.05$, *two-way ANOVA* **(B)** P2X2 immunofluorescence shows the localization of P2X2 (white) in the organ of Corti. The mid-modiolar sections of cochleae were harvested from pre-noise *Ocm*$^{+/+}$ and *Ocm*$^{-/-}$ mice at 3 - 4 wks of age. The red dashed box represents the OHC region, the red arrows point to the top of the OHC, and the yellow arrows show adjacent Deiters' cells. P2X2 receptor labeling was in the cell body of supporting cells and the straight phalangeal processes (yellow arrows). TM: tectorial membrane. **(C)** Maximum intensity projections of P2X2 immunolabeling on three rows of OHCs harvested from pre- and post-noise *Ocm*$^{+/+}$ and *Ocm*$^{-/-}$ mice. P2X2 (white), GCaMP6s (green), and DAPI (blue) are shown. Red arrows point to the OHC stereocilia. **(D, E)** Representative western blot for P2X2 protein expression levels detected in single cochlea derived from pre- or post-noise *Ocm*$^{+/+}$ and *Ocm*$^{-/-}$ mice at 3 - 4 wks. n = 3 for each genotype under each experiment condition, β-tubulin (loading control) was used for normalization, all values were then normalized to pre-noise *Ocm*$^{+/+}$. $p < 0.05$ *two-way ANOVA*, ns: not significant, *: $p < 0.05$; **: $p < 0.01$, *Bonferroni* post-test.

Figure 7 Differential rates of accelerated progressive hearing loss with the expression of GCaMP6s accelerated progressive hearing loss. Distortion product otoacoustic emissions (DPOAEs) were measured from GCaMP6s *Ocm*$^{-/-}$ mice and age-matched GCaMP6s *Ocm*$^{+/+}$ mice at **(A)** 3 - 4 wks, n = 10 *Ocm*$^{+/+}$ GCaMP6s- mice, n = 8 *Ocm*$^{+/+}$ GCaMP6s+ mice, n = 20 *Ocm*$^{-/-}$ GCaMP6s- mice and n = 7 *Ocm*$^{-/-}$ GCaMP6s+ mice, **(B)** 12 - 13 wks (n = 13 *Ocm*$^{+/+}$ GCaMP6s- mice, n = 7 *Ocm*$^{+/+}$ GCaMP6s+ mice, n = 6 *Ocm*$^{-/-}$ GCaMP6s- mice and n = 13 *Ocm*$^{-/-}$ GCaMP6s+ mice. $P < 0.0001$ for *Ocm*$^{+/+}$ vs. *Ocm*$^{-/-}$, and GCaMP6s- vs. GCaMP6s+, *three-way ANOVA*) and **(C)** 20 - 22 wks (n = 6 *Ocm*$^{+/+}$ GCaMP6s- mice, n = 10 *Ocm*$^{+/+}$ GCaMP6s+ mice, n = 6 *Ocm*$^{-/-}$ GCaMP6s- mice and n = 7 *Ocm*$^{-/-}$ GCaMP6s+ mice. $p < 0.0001$ for *Ocm*$^{+/+}$ vs. *Ocm*$^{-/-}$, and GCaMP6s- vs. GCaMP6s+, *three-way ANOVA*). **(D - F)** DPOAE threshold at 16 KHz at each age, black labels represent GCaMP6s-, green labels represent GCaMP6s+. Mean ± SD. $p < 0.05$ for 20 - 22 wks, *two-way ANOVA*, *: $p < 0.05$; **: $p < 0.01$; ***: $p < 0.001$, *Bonferroni* post-test.

References

Bienkowski, P., Scinska, A., Kostowski, W., Koros, E., & Kukwa, A. (2000). Ototoxic mechanism of aminoglycoside antibiotics--role of glutaminergic NMDA receptors. *Pol Merkur Lekarski*, *9*(52), 713-715. https://www.ncbi.nlm.nih.gov/pubmed/11144065 (Mechanizm ototoksycznego dzialania antybiotykow aminoglikozydowych--rola receptorow glutamatergicznych NMDA.)

Burnstock, G. (2016). P2X ion channel receptors and inflammation. *Purinergic Signal*, *12*(1), 59-67. https://doi.org/10.1007/s11302-015-9493-0

Ceriani, F., Hendry, A., Jeng, J. Y., Johnson, S. L., Stephani, F., Olt, J., Holley, M. C., Mammano, F., Engel, J., & Kros, C. J. (2019). Coordinated calcium signalling in cochlear sensory and non‐sensory cells refines afferent innervation of outer hair cells. *The EMBO journal*, *38*(9). https://doi.org/https://doi.org/10.15252/embj.201899839

Ceriani, F., & Mammano, F. (2012). Calcium signaling in the cochlea - Molecular mechanisms and physiopathological implications. *Cell Commun Signal*, *10*(1), 20. https://doi.org/10.1186/1478-811X-10-20

Chen, T.-W., Wardill, T. J., Sun, Y., Pulver, S. R., Renninger, S. L., Baohan, A., Schreiter, E. R., Kerr, R. A., Orger, M. B., Jayaraman, V., Looger, L. L., Svoboda, K., & Kim, D. S. (2013). Ultrasensitive fluorescent proteins for imaging neuronal activity. *Nature*, *499*(7458), 295-300. https://doi.org/10.1038/nature12354

Climer, L. K., Cox, A. M., Reynolds, T. J., & Simmons, D. D. (2019). Oncomodulin: The Enigmatic Parvalbumin Protein. *Front Mol Neurosci*, *12*, 235. https://doi.org/10.3389/fnmol.2019.00235

Climer, L. K., Hornak, A. J., Murtha, K., Yang, Y., Cox, A. M., Simpson, P. L., Le, A., & Simmons, D. D. (2021). Deletion of Oncomodulin Gives Rise to Early Progressive Cochlear Dysfunction in C57 and CBA Mice. *Front Aging Neurosci*, *13*, 749729. https://doi.org/10.3389/fnagi.2021.749729

Cox, B. C., Liu, Z., Lagarde, M. M. M., & Zuo, J. (2012). Conditional Gene Expression in the Mouse Inner Ear Using Cre-loxP. *Journal of the Association for Research in Otolaryngology*, *13*(3), 295-322. https://doi.org/10.1007/s10162-012-0324-5

Dallos, P. (1992). The active cochlea. *J Neurosci*, *12*(12), 4575-4585. https://www.ncbi.nlm.nih.gov/pubmed/1464757

Esterberg, R., Hailey, D. W., Coffin, A. B., Raible, D. W., & Rubel, E. W. (2013). Disruption of intracellular calcium regulation is integral to aminoglycoside-induced hair cell death. *J Neurosci*, *33*(17), 7513-7525. https://doi.org/10.1523/JNEUROSCI.4559-12.2013

Fernandez, E. A., Ohlemiller, K. K., Gagnon, P. M., & Clark, W. W. (2010). Protection against noise-induced hearing loss in young CBA/J mice by low-dose kanamycin. *J Assoc Res Otolaryngol*, *11*(2), 235-244. https://doi.org/10.1007/s10162-009-0204-9

Fridberger, Flock, Å., Ulfendahl, M., & Flock, B. (1998). Acoustic overstimulation increases outer hair cell Ca2+ concentrations and causes dynamic contractions of the hearing organ. *Proceedings of the National Academy of Sciences*, *95*(12), 7127-7132. https://doi.org/10.1073/pnas.95.12.7127

Fridberger, A., & Ulfendahl, M. (1996). Acute mechanical overstimulation of isolated outer hair cells causes changes in intracellular calcium levels without shape changes. *Acta Otolaryngol*, *116*(1), 17-24. https://doi.org/10.3109/00016489609137707

Fu, X., Wan, P., Li, P., Wang, J., Guo, S., Zhang, Y., An, Y., Ye, C., Liu, Z., Gao, J., Yang, J., Fan, J., & Chai, R. (2021). Mechanism and Prevention of Ototoxicity Induced by Aminoglycosides. *Front Cell Neurosci*, *15*, 692762. https://doi.org/10.3389/fncel.2021.692762

Hackney, C. M., Mahendrasingam, S., Penn, A., & Fettiplace, R. (2005). The concentrations of calcium buffering proteins in mammalian cochlear hair cells. *J Neurosci*, *25*(34), 7867-7875. https://doi.org/10.1523/JNEUROSCI.1196-05.2005

Hirose, K., & Liberman, M. C. (2003). Lateral wall histopathology and endocochlear potential in the noise-damaged mouse cochlea. *J Assoc Res Otolaryngol*, *4*(3), 339-352. https://doi.org/10.1007/s10162-002-3036-4

Hool, S. A., Jeng, J. Y., Jagger, D. J., Marcotti, W., & Ceriani, F. (2023). Age-related changes in P2Y receptor signalling in mouse cochlear supporting cells. *J Physiol*, *601*(19), 4375-4395. https://doi.org/10.1113/JP284980

Jeng, J.-Y., Carlton, A. J., Johnson, S. L., Brown, S. D. M., Holley, M. C., Bowl, M. R., & Marcotti, W. (2021). Biophysical and morphological changes in inner hair cells and their efferent innervation in the ageing mouse cochlea. *The Journal of Physiology*, *599*(1), 269-287. https://doi.org/https://doi.org/10.1113/JP280256

Jeng, J. Y., Ceriani, F., Hendry, A., Johnson, S. L., Yen, P., Simmons, D. D., Kros, C. J., & Marcotti, W. (2020). Hair cell maturation is differentially regulated along the tonotopic axis of the mammalian cochlea. *J Physiol*, *598*(1), 151-170. https://doi.org/10.1113/JP279012

Jeng, J. Y., Johnson, S. L., Carlton, A. J., De Tomasi, L., Goodyear, R. J., De Faveri, F., Furness, D. N., Wells, S., Brown, S. D., & Holley, M. C. (2020). Age‐related changes in the biophysical and morphological characteristics of mouse cochlear outer hair cells. *The Journal of Physiology*, *598*(18), 3891-3910. https://doi.org/ https://doi.org/10.1113/JP279795

Kidd Iii, A. R., & Bao, J. (2012). Recent advances in the study of age-related hearing loss: a mini-review. *Gerontology*, *58*(6), 490-496. https://doi.org/10.1159/000338588

Kujawa, S. G., & Liberman, M. C. (2006). Acceleration of age-related hearing loss by early noise exposure: evidence of a misspent youth. *J Neurosci*, *26*(7), 2115-2123. https://doi.org/10.1523/JNEUROSCI.4985-05.2006

Kujawa, S. G., & Liberman, M. C. (2009). Adding insult to injury: cochlear nerve degeneration after "temporary" noise-induced hearing loss. *J Neurosci*, *29*(45), 14077-14085. https://doi.org/10.1523/JNEUROSCI.2845-09.2009

Liu, J. P., Liu, S. C., Hu, S. Q., Lu, J. F., Wu, C. L., Hu, D. X., & Zhang, W. J. (2023). ATP ion channel P2X purinergic receptors in inflammation response. *Biomed Pharmacother*, *158*, 114205. https://doi.org/10.1016/j.biopha.2022.114205

Liu, X., Bulgakov, O. V., Darrow, K. N., Pawlyk, B., Adamian, M., Liberman, M. C., & Li, T. (2007). Usherin is required for maintenance of retinal photoreceptors and normal development of cochlear hair cells. *Proc Natl Acad Sci U S A*, *104*(11), 4413-4418. https://doi.org/10.1073/pnas.0610950104

Liu, Y., & Fechter, L. D. (1997). Toluene disrupts outer hair cell morphometry and intracellular calcium homeostasis in cochlear cells of guinea pigs. *Toxicol Appl Pharmacol*, *142*(2), 270-277. https://doi.org/10.1006/taap.1996.8059

Maison, S. F., Liu, X. P., Eatock, R. A., Sibley, D. R., Grandy, D. K., & Liberman, M. C. (2012). Dopaminergic signaling in the cochlea: receptor expression patterns and deletion phenotypes. *J Neurosci*, *32*(1), 344-355. https://doi.org/10.1523/JNEUROSCI.4720-11.2012

Mammano, F. (2011). Ca2+ homeostasis defects and hereditary hearing loss. *BioFactors*, *37*(3), 182 - 188. https://doi.org/10.1002/biof.150

Marcotti, W., & Kros, C. J. (1999). Developmental expression of the potassium current IK,n contributes to maturation of mouse outer hair cells. *The Journal of physiology*, *520 Pt 3*(Pt 3), 653-660. https://doi.org/https://doi.org/10.1111/j.1469-7793.1999.00653.x

Melgar-Rojas, P., Alvarado, J. C., Fuentes-Santamaria, V., Gabaldon-Ull, M. C., & Juiz, J. M. (2015). Validation of Reference Genes for RT-qPCR Analysis in Noise-Induced Hearing Loss: A Study in Wistar Rat. *PLoS One*, *10*(9), e0138027. https://doi.org/10.1371/journal.pone.0138027

Michna, M., Knirsch, M., Hoda, J. C., Muenkner, S., Langer, P., Platzer, J., Striessnig, J., & Engel, J. (2003). Cav1.3 (alpha1D) Ca2+ currents in neonatal outer hair cells of mice. *J Physiol*, *553*(Pt 3), 747-758. https://doi.org/10.1113/jphysiol.2003.053256

Mittal, R., Grati, M., Sedlacek, M., Yuan, F., Chang, Q., Yan, D., Lin, X., Kachar, B., Farooq, A., Chapagain, P., Zhang, Y., & Liu, X. Z. (2016). Characterization of ATPase Activity of P2RX2 Cation Channel. *Front Physiol*, *7*, 186. https://doi.org/10.3389/fphys.2016.00186

Mulvaney, J., & Dabdoub, A. (2012). Atoh1, an Essential Transcription Factor in Neurogenesis and Intestinal and Inner Ear Development: Function, Regulation, and Context Dependency. *Journal of the Association for Research in Otolaryngology*, *13*(3), 281-293. https://doi.org/10.1007/s10162-012-0317-4

Munoz, D. J., Thorne, P. R., Housley, G. D., & Billett, T. E. (1995). Adenosine 5'-triphosphate (ATP) concentrations in the endolymph and perilymph of the guinea-pig cochlea. *Hear Res*, *90*(1-2), 119-125. https://doi.org/10.1016/0378-5955(95)00153-5

Murtha, K. E., Yang, Y., Ceriani, F., Jeng, J. Y., Climer, L. K., Jones, F., Charles, J., Devana, S. K., Hornak, A. J., Marcotti, W., & Simmons, D. D. (2022). Oncomodulin (OCM) uniquely regulates calcium signaling in neonatal cochlear outer hair cells. *Cell Calcium*, *105*, 102613. https://doi.org/10.1016/j.ceca.2022.102613

Ohlemiller, K. K., Dahl, A. R., & Gagnon, P. M. (2010). Divergent aging characteristics in CBA/J and CBA/CaJ mouse cochleae. *J Assoc Res Otolaryngol*, *11*(4), 605-623. https://doi.org/10.1007/s10162-010-0228-1

Ohlemiller, K. K., & Gagnon, P. M. (2007). Genetic dependence of cochlear cells and structures injured by noise. *Hear Res*, *224*(1-2), 34-50. https://doi.org/10.1016/j.heares.2006.11.005

Orrenius, S., Zhivotovsky, B., & Nicotera, P. (2003). Regulation of cell death: the calcium–apoptosis link. *Nature Reviews Molecular Cell Biology*, *4*(7), 552-565. https://doi.org/10.1038/nrm1150

Pangrsic, T., Gabrielaitis, M., Michanski, S., Schwaller, B., Wolf, F., Strenzke, N., & Moser, T. (2015). EF-hand protein Ca2+ buffers regulate Ca2+ influx and exocytosis in sensory hair cells. *Proc Natl Acad Sci U S A*, *112*(9), E1028-1037. https://doi.org/10.1073/pnas.1416424112

Platzer, J., Engel, J., Schrott-Fischer, A., Stephan, K., Bova, S., Chen, H., Zheng, H., & Striessnig, J. (2000). Congenital deafness and sinoatrial node dysfunction in mice lacking class D L-type Ca2+ channels. *Cell*, *102*(1), 89-97. https://doi.org/10.1016/s0092-8674(00)00013-1

Richard, E. M., Maurice, T., & Delprat, B. (2023). Calcium signaling and genetic rare diseases: An auditory perspective. *Cell Calcium*, *110*, 102702. https://doi.org/10.1016/j.ceca.2023.102702

Schmittgen, T. D., & Livak, K. J. (2008). Analyzing real-time PCR data by the comparative C(T) method. *Nat Protoc*, *3*(6), 1101-1108. https://doi.org/10.1038/nprot.2008.73

Simmons, D. D., Tong, B., Schrader, A. D., & Hornak, A. J. (2010). Oncomodulin identifies different hair cell types in the mammalian inner ear. *J Comp Neurol*, *518*(18), 3785-3802. https://doi.org/10.1002/cne.22424

Telang, R. S., Paramananthasivam, V., Vlajkovic, S. M., Munoz, D. J. B., Housley, G. D., & Thorne, P. R. (2010). Reduced P2x2 receptor-mediated regulation of endocochlear potential in the ageing mouse cochlea. *Purinergic Signalling*, *6*(2), 263-272. https://doi.org/10.1007/s11302-010-9195-6

Thorne, P. R., Munoz, D. J., & Housley, G. D. (2004). Purinergic modulation of cochlear partition resistance and its effect on the endocochlear potential in the Guinea pig. *J Assoc Res Otolaryngol*, *5*(1), 58-65. https://doi.org/10.1007/s10162-003-4003-4

Tong, B., Hornak, A. J., Maison, S. F., Ohlemiller, K. K., Liberman, M. C., & Simmons, D. D. (2016). Oncomodulin, an EF-Hand Ca2+ Buffer, Is Critical for Maintaining Cochlear Function in Mice. *J Neurosci*, *36*(5), 1631-1635. https://doi.org/10.1523/JNEUROSCI.3311-15.2016

Vicente-Torres, M. A., & Schacht, J. (2006). A BAD link to mitochondrial cell death in the cochlea of mice with noise-induced hearing loss. *J Neurosci Res*, *83*(8), 1564-1572. https://doi.org/10.1002/jnr.20832

Wang, J. C., Raybould, N. P., Luo, L., Ryan, A. F., Cannell, M. B., Thorne, P. R., & Housley, G. D. (2003). Noise induces up-regulation of P2X2 receptor subunit of ATP-gated ion channels in the rat cochlea. *Neuroreport*, *14*(6), 817-823. https://doi.org/10.1097/00001756-200305060-00008

Wang, X., Zhu, Y., Long, H., Pan, S., Xiong, H., Fang, Q., Hill, K., Lai, R., Yuan, H., & Sha, S. H. (2018). Mitochondrial Calcium Transporters Mediate Sensitivity to Noise-Induced Losses of Hair Cells and Cochlear Synapses. *Front Mol Neurosci*, *11*, 469. https://doi.org/10.3389/fnmol.2018.00469

Yan, D., Zhu, Y., Walsh, T., Xie, D., Yuan, H., Sirmaci, A., Fujikawa, T., Wong, A. C., Loh, T. L., Du, L., Grati, M., Vlajkovic, S. M., Blanton, S., Ryan, A. F., Chen, Z. Y., Thorne, P. R., Kachar, B., Tekin, M., Zhao, H. B., . . . Liu, X. Z. (2013). Mutation of the ATP-gated P2X(2) receptor leads to progressive hearing loss and increased susceptibility to noise. *Proc Natl Acad Sci U S A*, *110*(6), 2228-2233. https://doi.org/10.1073/pnas.1222285110

Yang, H., Xie, X., Deng, M., Chen, X., & Gan, L. (2010). Generation and characterization of Atoh1-Cre knock-in mouse line. *Genesis*, *48*(6), 407-413. https://doi.org/10.1002/dvg.20633

Yang, Y., Murtha, K., Climer, L. K., Ceriani, F., Thompson, P., Hornak, A. J., Marcotti, W., & Simmons, D. D. (2023). Oncomodulin regulates spontaneous calcium signalling and maturation of afferent innervation in cochlear outer hair cells. *The Journal of Physiology*. https://doi.org/10.1113/jp284690

Yang, Y., Murtha, K., Climer, L. K., Ceriani, F., Thompson, P., Hornak, A. J., Marcotti, W., & Simmons, D. D. (2023). Oncomodulin regulates spontaneous calcium signalling and maturation of afferent innervation in cochlear outer hair cells. *J Physiol*, *601*(19), 4291-4308. https://doi.org/10.1113/JP284690

Zuo, H., Cui, B., She, X., & Wu, M. (2008). Changes in Guinea pig cochlear hair cells after sound conditioning and noise exposure. *J Occup Health*, *50*(5), 373-379. https://doi.org/10.1539/joh.l8032

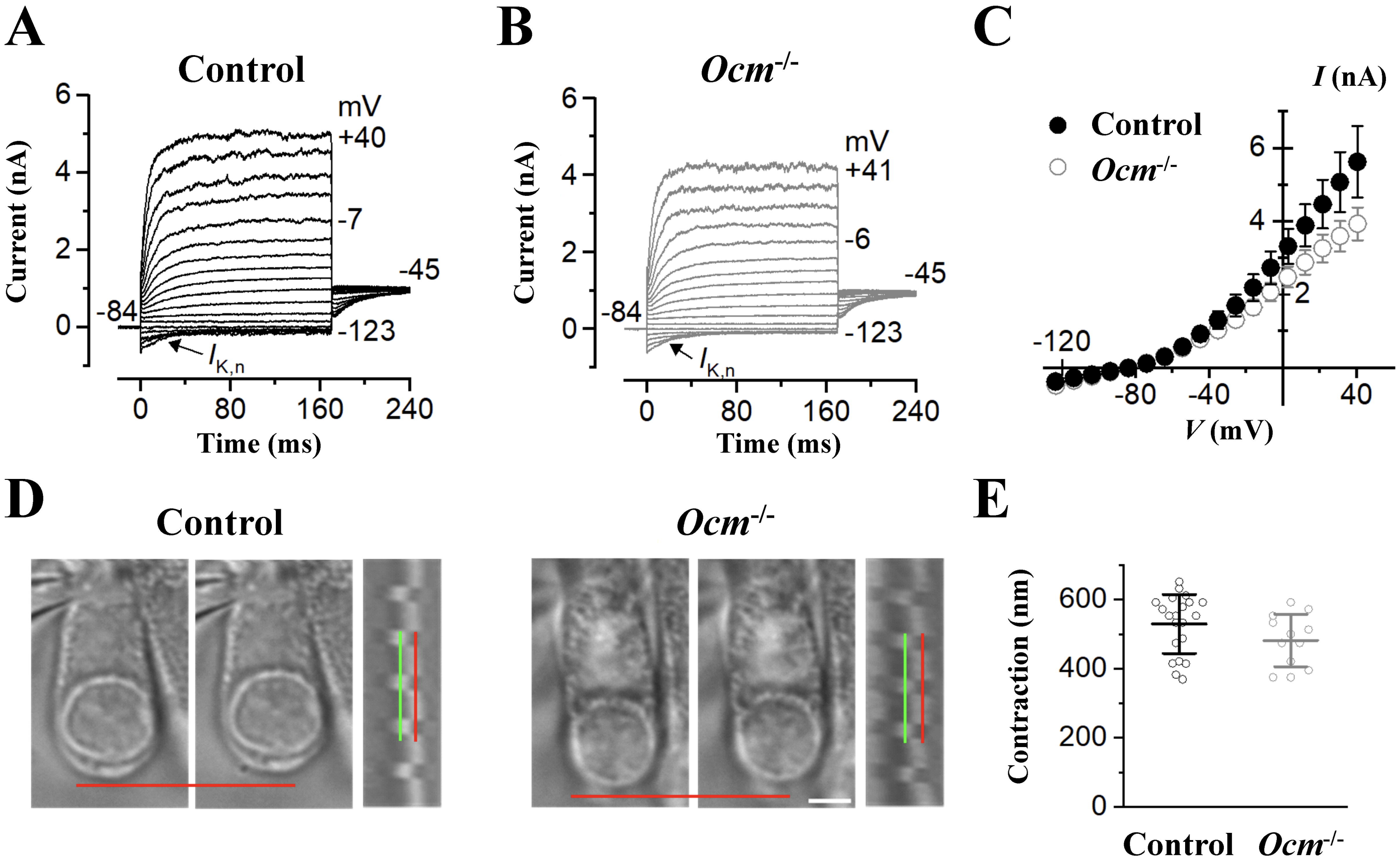
A
Control
6
4
2
0
Current (nA)
mV
+40
-7
-45
-84
-123
I_K,n
0
80
160
240
Time (ms)
B
Ocm-/-
6
4
2
0
Current (nA)
mV
+41
-6
-45
-84
-123
I_K,n
0
80
160
240
Time (ms)
C
I (nA)
Control
Ocm-/-
6
4
2
-120
-80
-40
40
V (mV)
D
Control
Ocm-/-
E
Contraction (nm)
600
400
200
0
Control
Ocm-/-

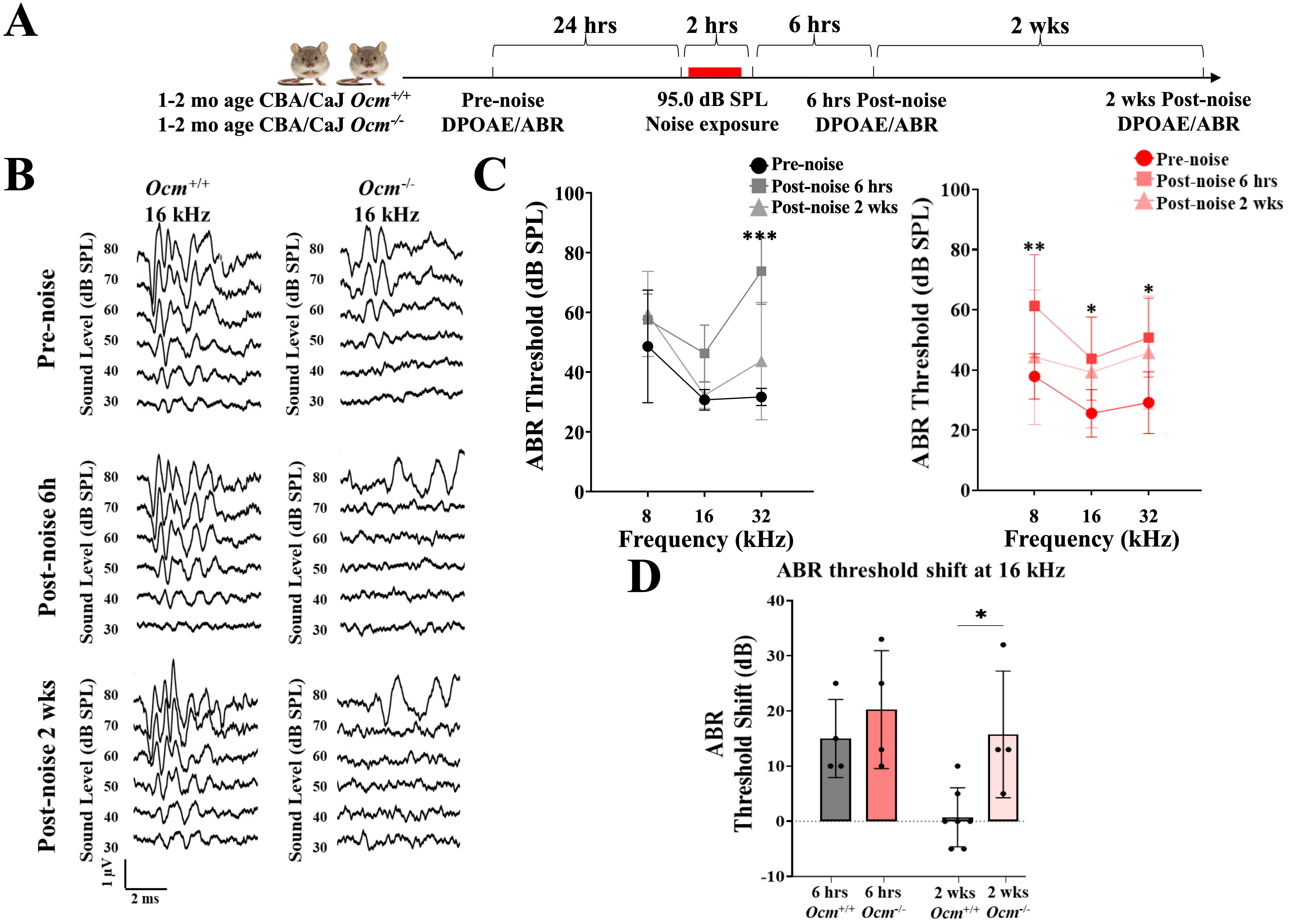
A
24 hrs
2 hrs
6 hrs
2 wks
1-2 mo age CBA/CaJ Ocm+/+
1-2 mo age CBA/CaJ Ocm-/-
Pre-noise DPOAE/ABR
95.0 dB SPL Noise exposure
6 hrs Post-noise DPOAE/ABR
2 wks Post-noise DPOAE/ABR
B
Ocm+/+ 16 kHz
Ocm-/- 16 kHz
Pre-noise
Post-noise 6h
Post-noise 2 wks
Sound Level (dB SPL)
80
70
60
50
40
30
1 µV
2 ms
C
Pre-noise
Post-noise 6 hrs
Post-noise 2 wks
ABR Threshold (dB SPL)
100
80
60
40
20
0
***
**
*
*
8
16
32
Frequency (kHz)
D
ABR threshold shift at 16 kHz
ABR Threshold Shift (dB)
40
30
20
10
0
-10
*
6 hrs Ocm+/+
6 hrs Ocm-/-
2 wks Ocm+/+
2 wks Ocm-/-

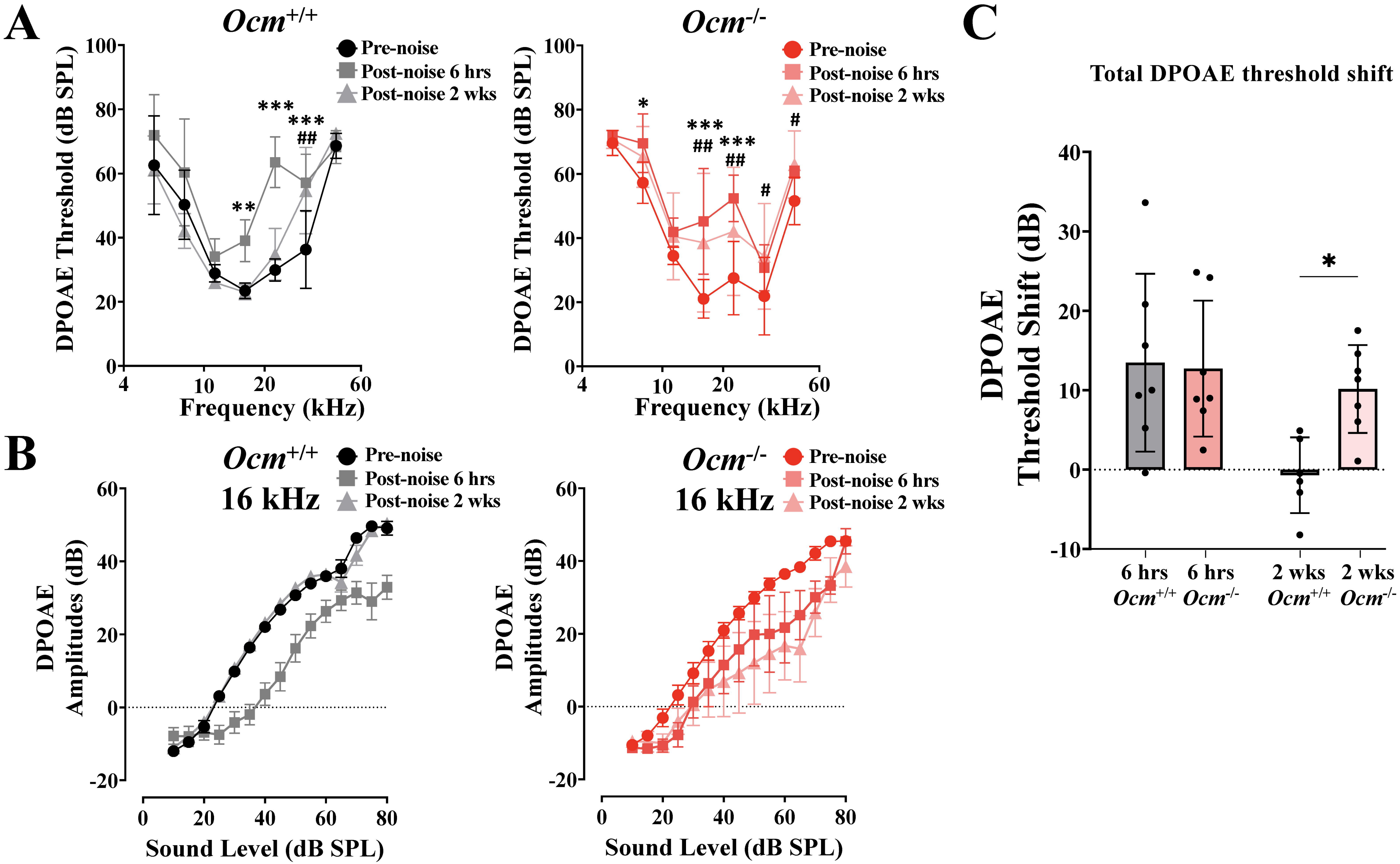
A
Ocm+/+
Pre-noise
Post-noise 6 hrs
Post-noise 2 wks
DPOAE Threshold (dB SPL)
100
80
60
40
20
0
4
10
20
60
Frequency (kHz)
**
***
***
##
Ocm-/-
*
***
##
***
##
#
#
B
Ocm+/+
16 kHz
DPOAE
Amplitudes (dB)
60
40
20
0
-20
0
20
40
60
80
Sound Level (dB SPL)
Ocm-/-
16 kHz
C
Total DPOAE threshold shift
DPOAE
Threshold Shift (dB)
40
30
20
10
0
-10
*
6 hrs
Ocm+/+
6 hrs
Ocm-/-
2 wks
Ocm+/+
2 wks
Ocm-/-

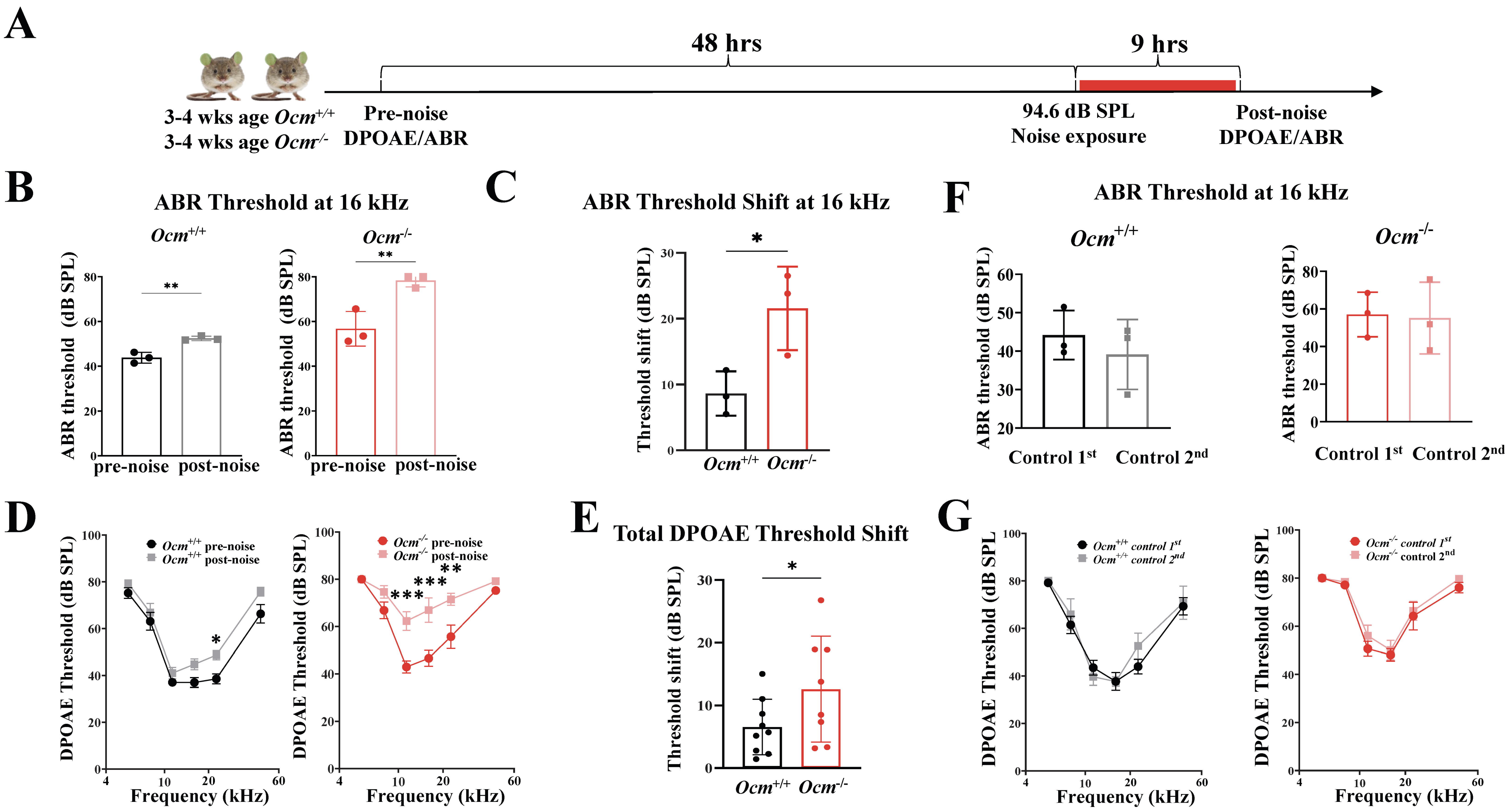
A
48 hrs
9 hrs
3-4 wks age Ocm+/+
3-4 wks age Ocm-/-
Pre-noise DPOAE/ABR
94.6 dB SPL Noise exposure
Post-noise DPOAE/ABR
B
ABR Threshold at 16 kHz
Ocm+/+
Ocm-/-
ABR threshold (dB SPL)
pre-noise
post-noise
**
C
ABR Threshold Shift at 16 kHz
Threshold shift (dB SPL)
Ocm+/+
Ocm-/-
*
F
ABR Threshold at 16 kHz
Ocm+/+
Ocm-/-
ABR threshold (dB SPL)
Control 1st
Control 2nd
D
DPOAE Threshold (dB SPL)
Ocm+/+ pre-noise
Ocm+/+ post-noise
Ocm-/- pre-noise
Ocm-/- post-noise
*
***
***
**
Frequency (kHz)
E
Total DPOAE Threshold Shift
Threshold shift (dB SPL)
Ocm+/+
Ocm-/-
*
G
DPOAE Threshold (dB SPL
Ocm+/+ control 1st
Ocm+/+ control 2nd
Ocm-/- control 1st
Ocm-/- control 2nd
Frequency (kHz)

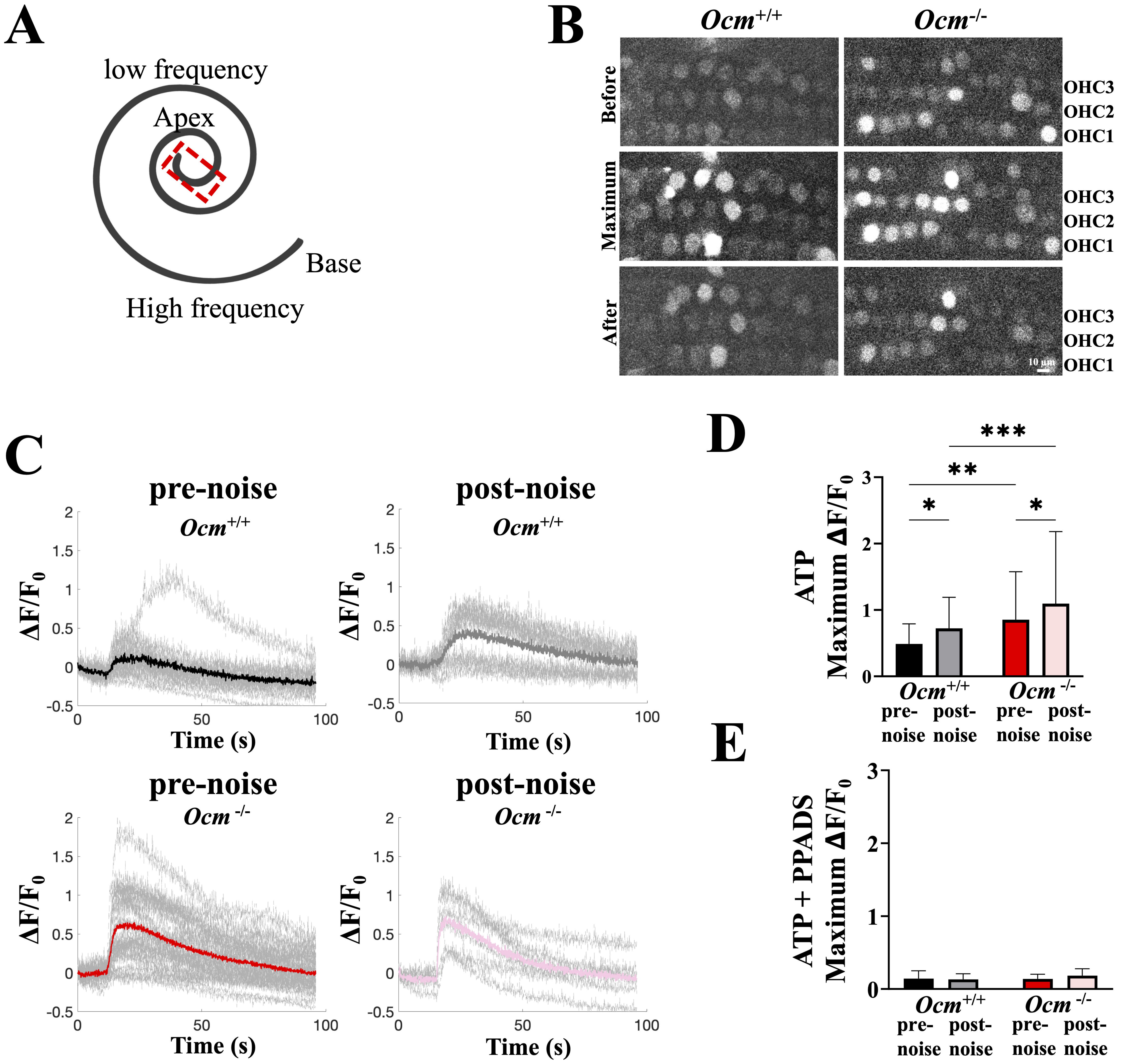
A
low frequency
Apex
Base
High frequency
B
Ocm+/+
Ocm-/-
Before
Maximum
After
OHC3
OHC2
OHC1
10 µm
C
pre-noise
Ocm+/+
post-noise
Ocm+/+
pre-noise
Ocm -/-
post-noise
Ocm -/-
ΔF/F0
Time (s)
2
1.5
1
0.5
0
-0.5
0
50
100
D
ATP
Maximum ΔF/F0
***
**
*
*
3
2
1
0
Ocm+/+
Ocm -/-
pre-noise
post-noise
pre-noise
post-noise
E
ATP + PPADS
Maximum ΔF/F0
3
2
1
0
Ocm+/+
Ocm -/-
pre-noise
post-noise
pre-noise
post-noise

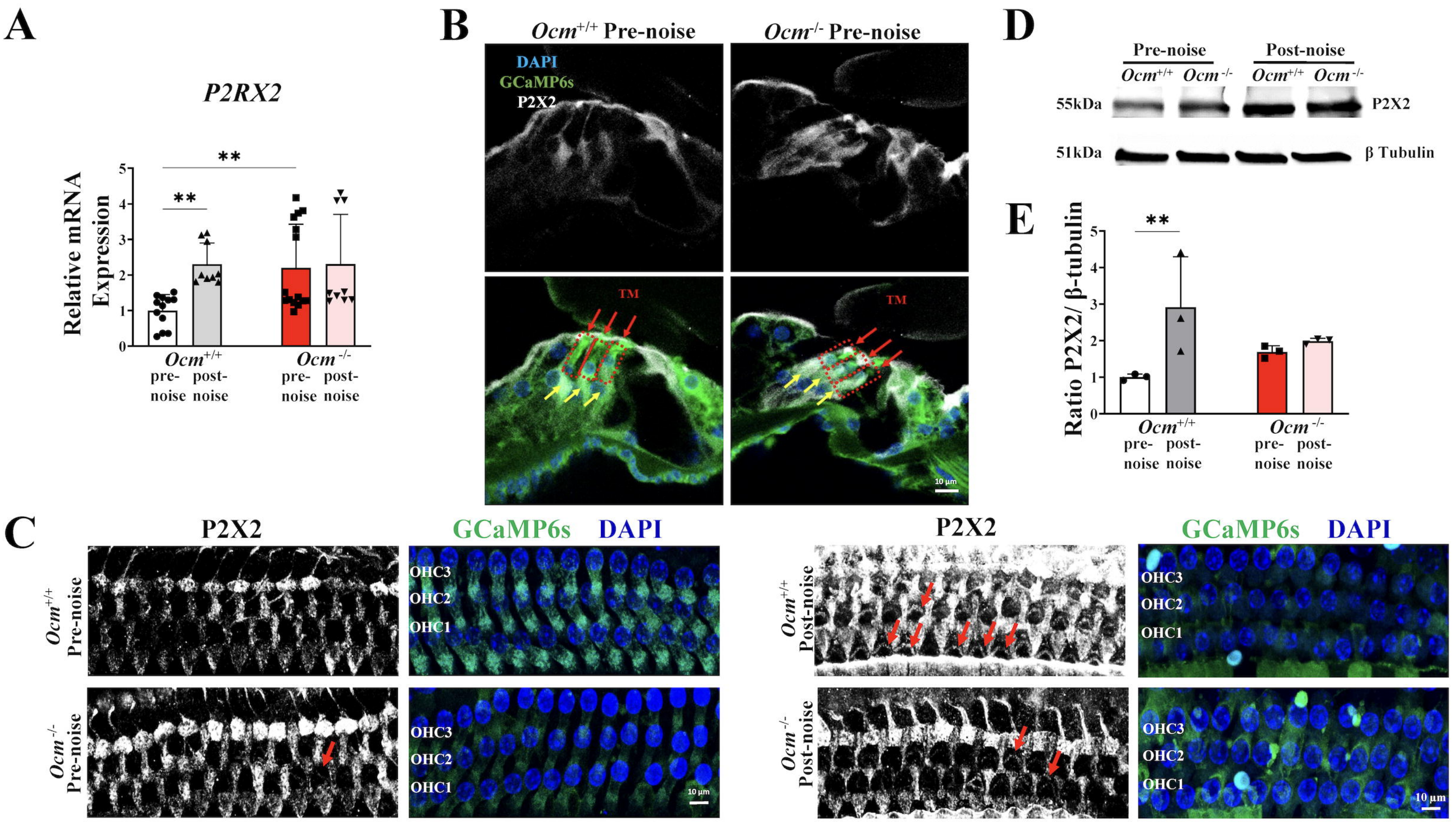
A
P2RX2
Relative mRNA Expression
0
1
2
3
4
5
**
**
Ocm+/+
pre-noise
post-noise
Ocm-/-
pre-noise
post-noise
B
Ocm+/+ Pre-noise
Ocm-/- Pre-noise
DAPI
GCaMP6s
P2X2
TM
TM
10 µm
C
P2X2
GCaMP6s DAPI
Ocm+/+ Pre-noise
Ocm-/- Pre-noise
OHC3
OHC2
OHC1
OHC3
OHC2
OHC1
10 µm
P2X2
GCaMP6s DAPI
Ocm+/+ Post-noise
Ocm-/- Post-noise
OHC3
OHC2
OHC1
OHC3
OHC2
OHC1
10 µm
D
Pre-noise
Post-noise
Ocm+/+
Ocm-/-
Ocm+/+
Ocm-/-
55kDa
P2X2
51kDa
β Tubulin
E
Ratio P2X2/ β-tubulin
0
1
2
3
4
5
**
Ocm+/+
pre-noise
post-noise
Ocm-/-
pre-noise
post-noise

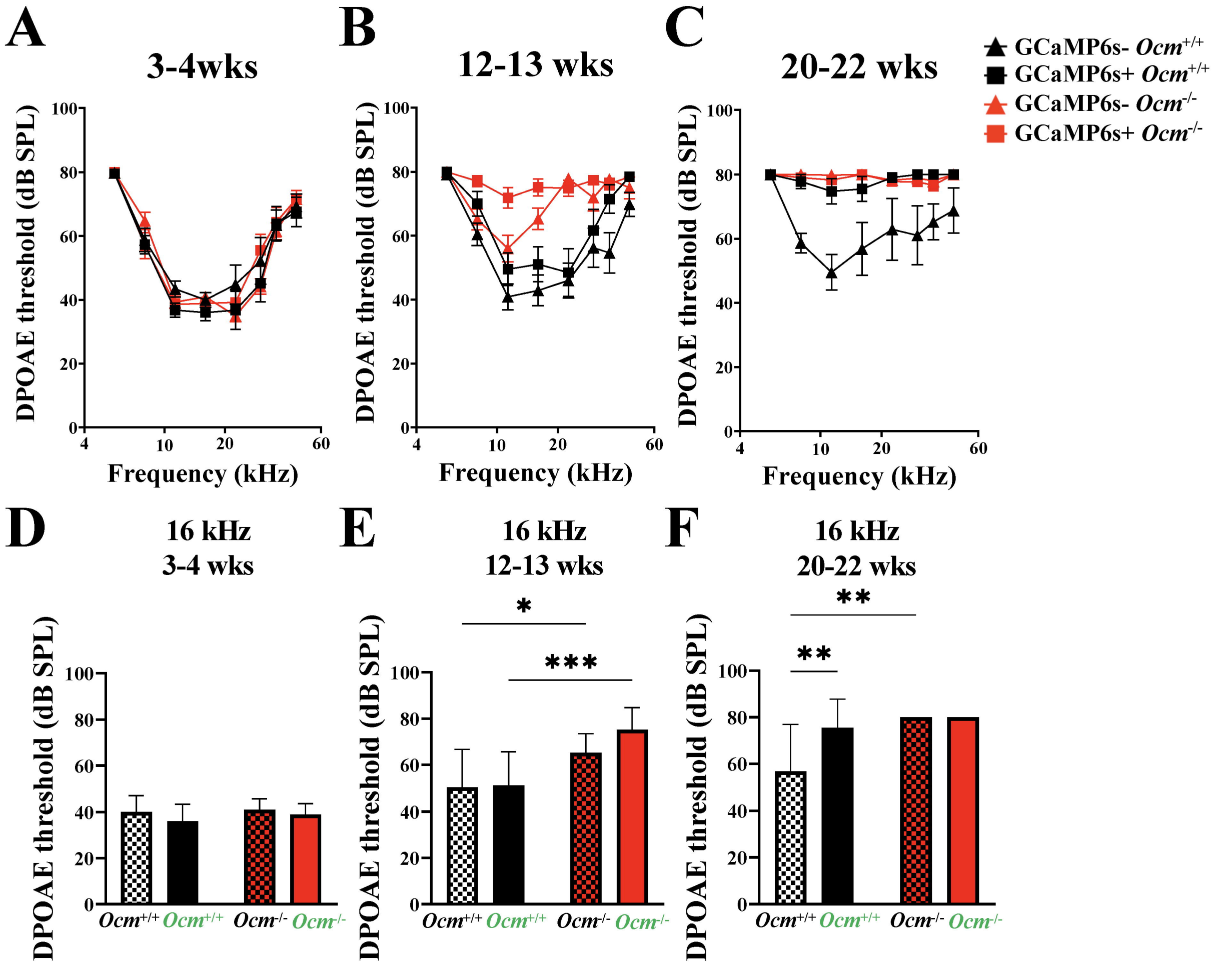
A
3-4wks
B
12-13 wks
C
20-22 wks
▲ GCaMP6s- Ocm+/+
■ GCaMP6s+ Ocm+/+
▲ GCaMP6s- Ocm-/-
■ GCaMP6s+ Ocm-/-
DPOAE threshold (dB SPL)
Frequency (kHz)
0
20
40
60
80
100
4
10
20
60
D
16 kHz
3-4 wks
E
16 kHz
12-13 wks
F
16 kHz
20-22 wks
*
***
**
**
Ocm+/+
Ocm+/+
Ocm-/-
Ocm-/-